Deep Learning Method for Quantitative Analysis of Covid -19 using CT Chest Images

Indrajeet Kumar
Graphic Era Hill University
Jyoti Rawat (drjyotirawat19@gmail.com)
Dehradun Institute of Technology: DIT University

Research Article

Keywords: Coronavirus, COVID-19, Neoplasm, Pandemic, Respiratory infection, Computed-Tomography, Deep learning

Posted Date: June 14th, 2021

DOI: https://doi.org/10.21203/rs.3.rs-540369/v1

Deep learning method for quantitative analysis of Covid-19 using CT chest images

I. Kumar, Ph.D[1] **J. Rawat, Ph.D[2]**

[1]Graphic Era Hill University, Dehradun, India. Email: drkumar5898@gmail.com

[2]DIT University, Dehradun, India. Email: drjyotirawat19@gmail.com

Abstract

The manual diagnostic tests performed in laboratories for pandemic disease such as COVID19 is time-consuming, requires skills and expertise of the performer to yield accurate results. Moreover, it is very cost ineffective as the cost of test kits is high and also requires well-equipped labs to conduct them. Thus, other means of diagnosing the patients with presence of SARS-COV2 (the virus responsible for COVID19) must be explored. A radiography method like chest CT images is one such means that can be utilized for diagnosis of COVID19. The radio-graphical changes observed in CT images of COVID19 patient helps in developing a deep learning-based method for extraction of graphical features which are then used for automated diagnosis of the disease ahead of laboratory-based testing. The proposed work suggests an Artificial Intelligence (AI) based technique for rapid diagnosis of COVID19 from given volumetric CT images of patient's chest by extracting its visual features and then using these features in the deep learning module. The proposed convolutional neural network is deployed for classifying the infectious and non-infectious SARS-COV2 subjects. The proposed network utilizes 746 chests scanned CT images of which 349 images belong to COVID19 positive cases while remaining 397 belong negative cases of COVID19. The extensive experiment has been completed with the accuracy of 98.4 %, sensitivity of 98.5 %, the specificity of 98.3 %, the precision of 97.1 %, F1score of 97.8 %. The obtained result shows the outstanding performance for classification of infectious and non-infectious for COVID19 cases.

Keywords: Coronavirus, COVID-19, Neoplasm, Pandemic, Respiratory infection, Computed-Tomography, Deep learning.

1. INTRODUCTION

The novel coronavirus first encountered at Wuhan, China has been designated as SARS-COV2 i.e. severe acute respiratory syndrome Coronavirus 2, while the disease it causes is termed as COVID19 (Corona Virus Disease 2019) [1-2]. Coronavirus is a family of various viruses which affects humans, animals or both. In humans, various coronaviruses can cause diseases ranging from an acute illness like common cold to severe illnesses like SARS (Severe Acute Respiratory Syndrome) and MERS (Middle East Respiratory Syndrome) [3]. SARS-COV2 has "club-shaped" projection overs its spherical envelope which is also called spike glycoprotein and also possesses positive sense ssRNA (Single-stranded RNA) within its nucleocapsid. Coronaviruses are known to have 26kb -32 kb genomes which are the largest genome for RNA dominant viruses while their G+C contents range 32 to 43%. These genomes consist of a unique N-terminal fragment inside its spike and various other types of features as mentioned in [4-5]. SARS and

MERS viruses namely SARS-CoV and MERS-CoV respectively are known to cause symptoms like cough, fever and breathlessness in its patients. Patients with SARS can also be effects by severe respiratory problems and are prone to a higher fatality rate as compared to other coronaviruses. Various research suggests that the origin of MERS-Cov and SARS-CoV is from bats but spread to human from different medium like SARS-CoV spread to human from civets whereas MERS-CoV spread from dromedaries. Likewise, SARS-CoV2 is also speculated to be spread from bats while the source of spread is still unclear [6].

The outbreak of uncommon and human-to-human contagious respiratory illness also call COVID19 caused by SARS-CoV2 has been termed as a pandemic by WHO (World Health Organization) as it has affected a total of 210 countries with a majority of cases from the USA, Italy, Russia, United Kingdom, China, Brazil, India etc. [3, 8] and 164,909,681 overall cases reported till May 18, 2021, out of which 3,418,998 people have lost their lives while 143,884,736 have recovered. The contagiousness of the novel coronavirus is highest among other coronaviruses as suggested by R0 metric, on average, an infectious human can spread the virus to about 3 other healthy humans [3, 7]. Thus, it is important to diagnose the patients suffering from COVID19 and then quarantine them for isolated monitoring and treatment. It is also observed that patients with compromised immunity due to medical history have higher fatality rate to the virus than other patients which makes early diagnosis and isolation more crucial to safeguard them especially the cancer patients who have twice more risk of getting infected than the normal person.

The patients with COVID19 can be diagnosed using various criteria i.e., symptoms, epidemiology, CT images and pathology test. The symptoms of COVID19 contains cold, cough, fever, pneumonia and other respiratory discomforts [9-11]. However, the above-mentioned symptoms might not be the specific COVID19 symptoms as there are many reports of asymptomatic patients tested positive through chest CT images as well as pathological test. A person under investigation (PUI) is subjected to laboratory-based pathological test by extracting a sample like bronchoalveolar lavage, sputum or tracheal aspirate from the lower respiratory system. This laboratory test is an RT-PCR(*Reverse transcription-polymerase chain reaction*) and nucleic acid sequencing of the virus' RNA [12] and since the outbreak is observed, the diagnosis against the COVID19 has been affected by various factors like availability, accuracy, quality, efficiency as well as the cost of these testing kits that have caused the tremendous increase in the spread of the virus as an infectious person may observe the symptoms of the virus two weeks after getting infected while he/she can still spread it to people coming in contact [13]. Moreover, the accuracy of the virus depends upon nucleic acid extraction methods, disease stages, sample collection, and on the expertise of the sample collector or human errors. The rate of detection of nucleic acid is found to be in range to 30-50% [14] and thus repetitive testing is done to confirm the diagnosis. The radiological methods like CT scan can also be utilized for diagnosing COVID19 with more accuracy by utilizing the CT image features such as peripheral lung distribution and lung morphology, or other features like pulmonary consolidation, ground-glass opacities from late and early stage of COVID19 respectively [15]. However, there are also possibilities of these CT images being similar to patients of other infectious diseases like pneumonia [16-18].

Artificial Intelligence-based techniques like deep learning are developed to deal with problems like feature extraction and classification by utilizing medical images. These features may include shape-based or spatial features which are efficiently used to distinguish between the infectious and non-infectious individuals. There are various numbers of other features that can also be used for detecting pathogens by pattern analysis from input image associated with the pathogenesis [21]. CNN (Convolutional Neural network) is one such deep learning-based network which has been used to enhance the low-intensity images from given video endoscopy even with a small dataset of 55 videos [19]. CNN can also detect pneumonia using X-ray images, the nature of pulmonary swellings using CT images, or cyst from endoscopic videos [17-20]. The chest CT images of COVID19 patients in their early stages are observed to contain ground glass-opacity in one of the lungs which later progresses to both of them [22]. Similar features can also be observed in the pneumonic patients with little differences which are difficult to identify by the radiologist but can be observed by using artificial intelligence techniques like CNN.

The RT-PCR standard diagnosis was initially reported with 30-70% sensitivity while at that time the CT diagnosis was more sensitive but the recent data from US labs from the University of Washington suggests that the next generation COVID19 RT-PCR diagnosis 95 % or more sensitivity. Even after being more sensitive than RT-PCR in earlier days of the outbreak, CT images were never used for COVID19 diagnosis. Various US-based radiology society has suggested to use CT cautiously and only during the time when the diagnosis is harder to manage through pathology while there will certainly be cases where CT imaging is needed for other reasons but the presence of SARS-CoV2 is observed [1-2]. Thus, healthcare professionals need to be familiar with various imaging features of the infection. Usually, a patient with symptoms related to COVID-19 such as shortness of breath, fever or cough is made to take chest X-RAY. The most common abnormalities of such patients involve ground glass opacities which look like frosted glass. However, it is observed that the X-rays are not much sensitive to COVID19 and can result in false-negative diagnosis whereas CT images of the chest are more detailed and distinguishable as compared to X-ray images. The common abnormalities in case of CT images are ground-glass opacities scattered throughout the lungs that are observed due to liquid filling of alveoli. In severe infections, more fluid accumulates inside the lobes of the lungs making the ground-glass appear like solid white consolidation which in certain cases is further observed as “crazy paving” pattern formed due to swelling of lung lobules present along with the interstitial space. These results in walls appear similar to irregularly shaped stones used to pave a street, hence the name “crazy paving” [21-22].

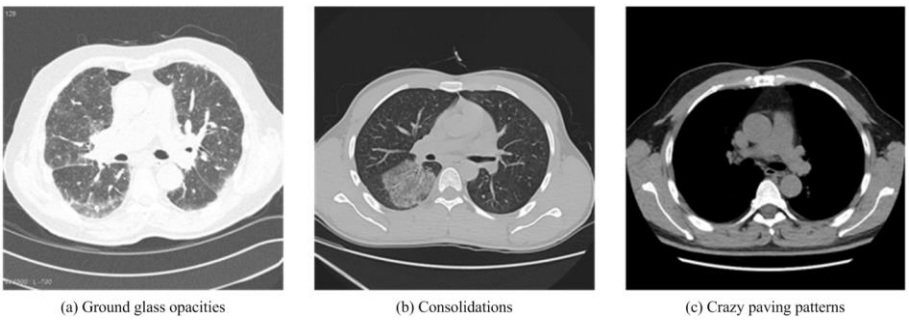

Fig. 1 Basic CT findings: (a) Ground glass opacities, (b) Consolidations and (c) Crazy paving patterns [46].

The three CT observations i.e., crazy paving patterns, consolidations and ground-glass opacities may be detected in isolation or combination with one another as shown in **Fig. 1**. Usually, ground glass is first to sign to appear and later followed by one or both of the other occurring in multiple lobes inside both lungs in severe patients while in mild infections the ground glass opacity can be present within one lobe. Thus, it can be said that the severity of the disease depends upon the proportion of lung findings which may or may not be observed in COVID19 patient. Moreover, the recovery of the patient can also be monitored in quantitative manner through CT imaging which is not provided by any other test. Some other findings like pleural effusions or fluid inside the lungs can also be observed in CT imaging, which is common in patients with bacterial pneumonia and congestive heart failure [1]. These observations in CT imaging namely crazy paving patterns, consolidations and ground-glass opacities can also be found in various types of viral pneumonia-like influenza and adenovirus, and other non-infectious illnesses. This implies that CT is not specifically sensitive to COVID19 and thus patients with these findings should get further clinical evaluation and laboratory test done to confirm the presence of the virus. It is recommended to utilize the CT imaging in case of unavailability of pathological testing as it can correctly identify the true negative cases but for confirming true positive cases it needs further testing. Individuals presenting to hospital with above-mentioned chest findings may need isolation and should get comprehensive confirmatory testing and required treatment [2]. The major symptoms of the development of COVID-19 in human body are shown in **Fig. 2**.

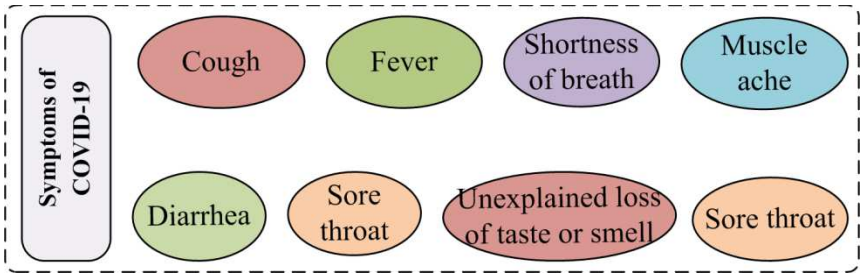

Fig. 2 Major symptoms of the development of COVID-19 [1-2].

After the study of past statistics [1-2] and **Fig. 2**, it is observed that in rare cases, COVID-19 can lead to severe respiratory problems, kidney failure or death. It is also observed that the findings CT images are not specific to COVID19 only and there are some cases which are suspected as COVID-19 but have a pattern on CTE that is consistent with acute lung injury, various types of viral pneumonia (influenza A, influenza B, RSV, Coronavirus, rhinovirus, parainfluenza, and adenovirus), some atypical bacteria types of pneumonia (legionella, mycoplasma), drug-induced acute lung injury (chemotherapy, immunotherapy) and cryptogenic organizing pneumonia which is an idiopathic form of primary organizing pneumonia. **Table 1** explains the basic CT finding characteristics.

Table 1 The CT findings

	Early CT findings		Late CT findings
1	Bilateral peripheral ground glass opacities (often rounded morphology)	1	Confluent ground glass opacity
2	With or without superimposed consolidation	2	Crazy paving
3	No discrete nodules	3	Superimposed consolidation
4	No pleural effusion	4	Linear opacities
5	No lymphadenopathy	5	Architectural distortion and Bronchiolar dilation

There are some early CT findings related to viral pneumonia which appear to be dominated by bilateral peripheral ground-glass opacities. These ground-glass opacities possess round morphology which is not due to swellings or nodules found in the lungs. The consolidation can be superimposed on the ground glass opacities, but early CT findings do not contain many cases of consolidation as compared to ground-glass opacities, also in early cases discrete nodules, pleural effusion and lymphadenopathy are not reported. Among these, the pleural effusions and lymphadenopathy are not characteristic of the disease. With the progress of the disease, the ground-glass opacity becomes more confluent and often remains denser in lungs periphery but is also present throughout the lungs, in severe cases crazy paving is observed. There's also a report of linear opacities developing later in the disease process and those linear opacities being associated with architectural distortion. Also, within the areas of opacification, bronchiolar dilation is observed that may not be anywhere else in the lung [23]. The proportion of mild and asymptomatic cases versus acute and lethal cases is shown in **Fig. 3**.

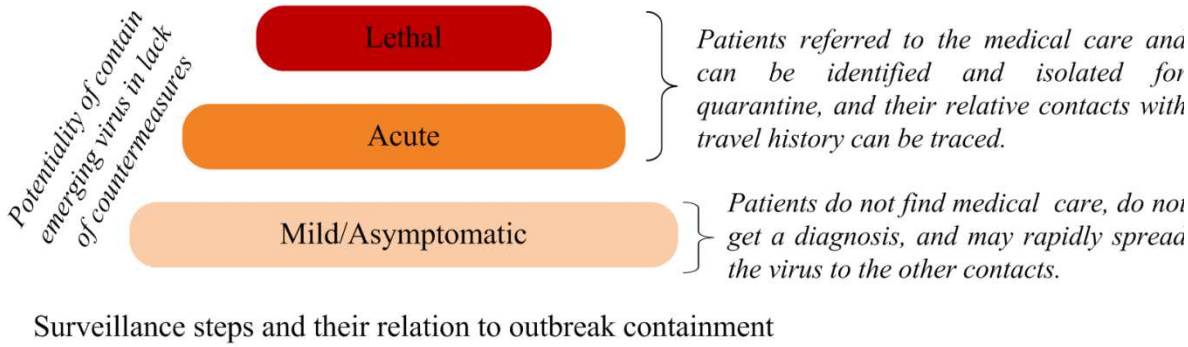

Fig. 3. The major surveillance steps and their relation to COVID-19 containment [3].

The present work aims to study the results yielded by implementing deep learning-based CNN for detecting the presence of SARS-COV2 from given CT images. The present implementation uses a total of 349 images containing both the COVID19 as well as viral pneumonia cases. The remainder sections of the paper consist of following sections: "Literature review" which describes the current literature associated with COVID19, "Proposed model" section offers a detailed structure of the proposed classification model, "Performance analysis" focuses on the analyses of results

obtained in comparison to the global standards and finally "Conclusion" section contains the statements which can be inferred from the present work.

LITERATURE REVIEW

The preparedness for COVID19 in countries with exponentially increasing cases have emphasized the need for quick diagnosis, containment as well as contact tracing [24]. As the contiguousness of virus is extremely high, the nucleic acid-based RT-PCR test can be made more efficient and reliable through other diagnostic techniques so as to deal with false-negative results, such techniques involve CT imaging-based techniques which were included in diagnosis in China during the early outbreak. The abnormality detected in CT imaging predates RT-PCR in asymptomatic as well as symptomatic patients who were later diagnosed with COVID19 [25-26]. However, certain patients with COVID19 positive diagnosis had no findings in CT imaging which likely shows an early infection, data shows that of 36 patients who were scanned within 2 days of showing symptoms, about 90% were tested positive for COVID19 through RT-PCR but about 56%patients had no CT findings [27]. The three CT observations i.e., crazy paving patterns, consolidations and ground-glass opacities may be detected in isolation or in combination with one another in patients with COVID19 pneumonia [25, 27–30].

The work conducted in [30] involved 1014 patients who were subjected to both types of testing i.e., RT-PCR and CT, the sensitivity related to CT imaging is found to be 97% of RT-PCR positive cases. The 81% of patients who were diagnosed negative through RT-PCR but found positive through CT were reassigned as "probable" by analyzing their clinical symptoms. The differences in bacterial or other viral pneumonia and COVID19 related pneumonia are being currently studied [31]. The crazy paving pattern is likely to be observed within 4-14 days period after the symptoms are experienced by the patients while other observations like large volume lymphadenopathy, cavitation, cysts, nodules and tree-in-bud pattern, are rarely found. CT imaging is certain to become important for diagnosing the presence of COVID19 related pneumonia in patients. Moreover, the evolution of pneumonia in patients with COVID19 along with their recovery can be easily observed through regular monitoring of CT images 2 days after the symptoms are reported. It is also reported that patients with no presence of COVID19 in CT images taken a week after experiencing symptoms are unlikely to develop pneumonia related to the virus. As the pandemic is progressing, various new data and studies are being put forward from different affected regions on a daily basis which can help in knowing other features which are specific to COVID19.

The British Society of Thoracic Imaging issued guidelines for the assessment of COVID19 suspected cases through laboratory, clinical as well as radiography and advised to reserve CT imaging for severe patients and during diagnostic uncertainty. It is also reported that in certain cases the sensitivity of CT is found to be higher than RT-PCR. RT-PCR related test requires deep throat swab or throat wash sample for detecting SARS-CoV2 and is a state-of-art testing method for the virus whereas CT imaging provides results that are suggestive for further diagnosis. The CT morphology that depends upon various features of COVID19 patients can be helpful in diagnosis especially in the case of false-negative result yielded by RT-PCR [31]. The author in [32] measured various features associated with COVID-19 from a dataset containing CT images of infectious and non-infectious patients from the place Iran and

draws the hypothesis that some CT features have short-term predictive value. Pleural effusions and sub-pleural sparing are observed in one-sixth and one-fifth of COVID-19 positive patients respectively. They Studied the initial group of Iranian patients from Kashan, a hotspot of COVID-19 in Iran and also examined the features related to COVID-19 based pneumonia. The above-mentioned study [32] was conducted on low-dose CT imaging protocol designed for potential COVID-19 based pneumonia.

A study [31] indicated that peripheral distribution, GGO and vascular thickening are among most distinctive CT imaging features related to COVID-19 and necessary negative features involved in the study are hilar/mediastinal lymphadenopathy, cavitation and lack of tree-in-bud nodules. A study [32] indicates the presence of mild splenomegaly in various viral diseases which is not mentioned in earlier studies of COVID-19. There were 6 patients with normal initial CT image who were asymptomatic and came in contact with confirmed COVID-19 patients. This data emphasizes the need for using RT-PCR along with CT imaging for proper monitoring of patients' condition or recovery. The patients with severe conditions or those who lost their lives because of pneumonia related to COVID-19 are found to be considerably older and their CT findings had more crazy-paving and consolidation pattern, the involvement of peri-bronchovascular, pleural effusion and developed air bronchograms. Thus, the radiology-based feature can be utilized to describe prognostic imaging biomarkers of pneumonia related to COVID-19.

The unstable or severe patients also show involvement of peri-bronchovascular along with the subpleural distribution found in the periphery of the lungs while the stable patients are found to show perilobular opacity and RHS (reverse halo sign) [32-34]. Moreover, the severe, as well as the deceased patients, were found to have a higher frequency of pleural effusion, though these findings are non-COVID-19 specific and were reported by [35]. The time of taking CT scan and severity of disease are the factors affecting the findings of radiology, it is reported that in mild or acute symptomatic patients about 18% of total patients had normal CT images while only 3% of total patients had normal initial findings that later developed severe illness [36-38]. A study [37] described radiological findings in subclinical disease showing GGO in CT images of 15 patients taken before the symptoms are encountered. The sudden surge of COVID-19 cases in Hubei province of China on 12 February 2020 led to a shortage of testing kits and also due to time constraint, CT imaging was found to be a reliable and efficient method for diagnosis in such scenario. This helped in taking timely measures to contain the disease and treat the patients; however, the possibility of false-negative due to CT imaging taken in the early stage of the disease cannot be ignored [39-40].

A study [41] observed the rate of misdiagnosis of COVID-19 by the radiologists and found that in a sample of 51 patients, the CT features of COVID-19 were overlapping with that of infection caused by adenovirus. These overlapping involved similarities as well as dissimilarities with the CT imaging-based features of SARS (severe acute respiratory syndrome). The false-negative cases recorded through CT scan were found to be just 3.9% (2/51) and suggests CT imaging as a potential method for testing. A study [42] conducted for pediatric patients used CT as well as the laboratory-based test of 20 such patients of which 65% had contact with already positive COVID-19 family members, cough and fever were common symptoms recorded by 65% and 60% of them respectively. The features related to CT scans involved coinfection in 40%, pulmonary lesions in 30%, bilateral pulmonary lesions in 50%, 20% with no findings and 80% with procalcitonin elevation (not common among adults). A deep-learning-based technique

called COVNet (COVID19 detection neural network) had been developed for extracting the features from CT images of patient's chest and then used for diagnosing the presence of COVID19 in that patient [43-44].

The CT images of non-pneumonia and CAP (Community-acquired pneumonia) are analyzed for determining the effectiveness of the model. It involves dataset taken from 6 hospitals and performance analysis of the model is done through specificity, sensitivity and AUC (Area Under curve) associated with operating characteristics of the receiver [43]. The dataset contains 4,356 CT images obtained from 3,322 patients. The specificity and sensitivity on per-exam basis for diagnosis of COVID19 is found to be 294 of 307 (96% [95% CI: 93%, 98%]) and 114 of 127 (90% [95% CI: 83%, 94%]) respectively, while AUC is found to be 0.96 (p-value<0.001) [43]. In a study [45], a CNN (Convolutional Neural Network) based technique is used for classifying the CT image as COVID19 positive, viral pneumonia, influenza or normal. A comparison is done with results of CNN and other 3D and 2D deep learning-based models. The CNN based model was able to yield specificity and sensitivity of 92.2 and 98.2% respectively [45].

From the above state of the art, it is summarized that there is very less number of work that analyzed CT imaging technique with the implementation of deep learning methods for detecting COVID-19 features. So, the aim is to analyze the results yield by implementing deep learning-based CNN to detect the presence of COVID-19 from given CT images that can be utilized for diagnosing the potential patients more efficiently and reliably.

3. MATERIAL AND METHODS

Accurate detection of COVID19 is a challenging task for all the experts of the medical fraternity. Therefore, in this work a computer assisted system has been proposed for analysis and classification of COVID19 cases using CT images and deep learning method. The description of dataset, proposed model, experiments and results are discussed here.

3.1 Database description

CT scans can prove to be vital mode of COVID19 diagnosis to provide fast, accurate and cheap and more feasible way for its screening and testing. In this paper, a dataset used for implementing the proposed technique contains 746 chest CT images taken from 143 patients with average age of 49±15 years and 2 classes namely (1) class 1: infectious i.e., CT images having positive report for COVID19 and (2) class 2: non-infectious i.e., CT images having negative report for COVID19. A total of 480 images of given dataset were used for training set, 80 images of given dataset is used as a validation set while 186 remaining images were utilized for testing set. The data is available at https://github.com/UCSD-AI4H/COVID-CT [46].

3.2 Overview of the proposed architecture

The proposed work consists of three major sections as pre-processing section, model building section and decision-making section. Each section consists of a set of processes and each process is very helpful in getting the desired results. The experimental workflow diagram of the proposed system is shown in **Fig. 4**.

Step involved in proposed work is given as:

Step 1 Load input CT scan images.

Step 2 Resize all the images into 224 × 224 × 3 for similar size and equal to input layer size of proposed deep learning model.

Step 3 Remove the patient information from input CT images and reduce the noises if there is any kind of noise or artifact.

Step 4 All preprocessed images are divided into training, validation and testing set in the ratio of 65:10:25.

Step 5 Training set is applied on defined model with stochastic gradient descent kernel function and different combination of defined Identity Blocks i.e., IB-1 & IB-2.

Step 6 On the trained model, testing set is applied, and results are obtained.

Step 7 Lastly, performance evaluating parameters are computed for total testing set.

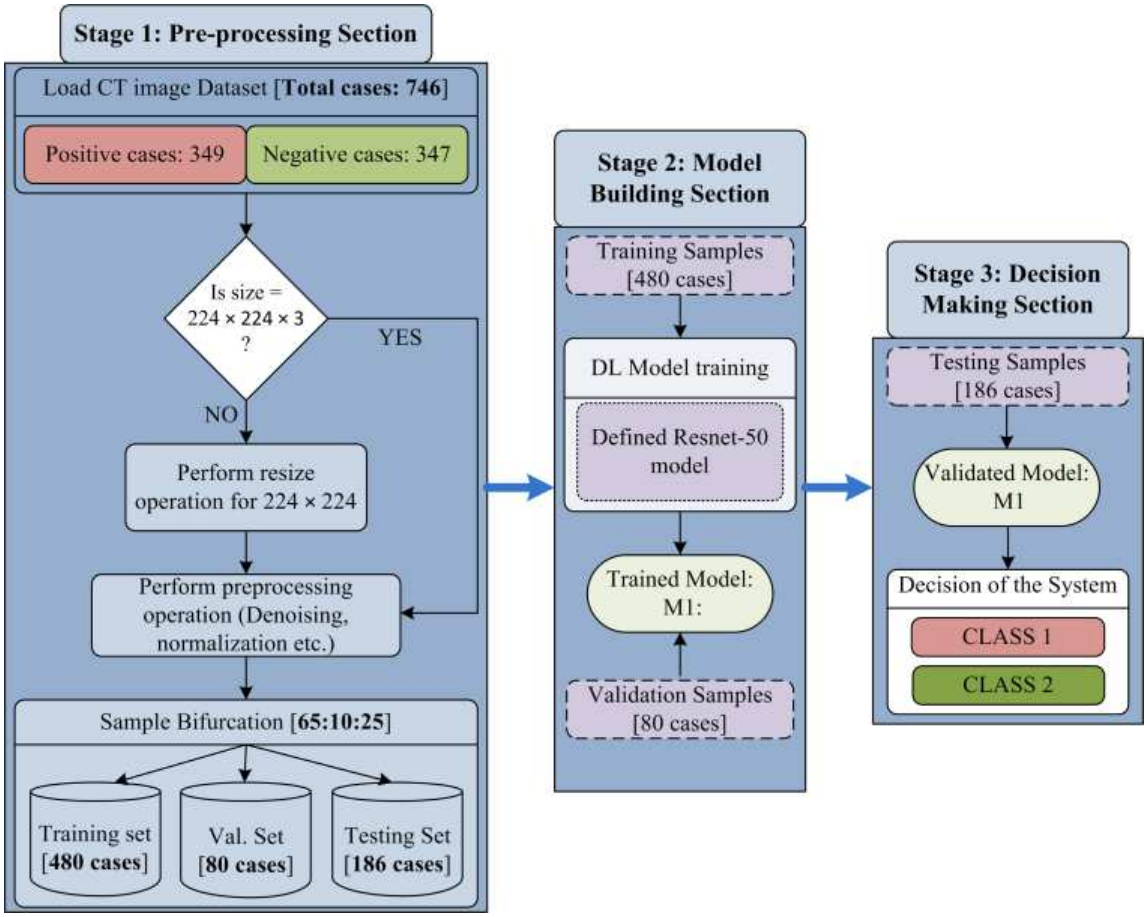

Fig. 4. Experimental Workflow Diagram of Proposed Model

3.2.1 Pre-processing Section

The first section of the designed model is the preprocessing section, in which the input CT scan images are loaded. The CT scan images of collected dataset are generated from different types of CT scanners having different features, due to this there are so many variations in image resolution. It is also known that the variations in input data size can be very big constraint for the development of any high performing system. Therefore, all input images are resized to 224 × 224 pixels. Another important part of preprocessing section is de-noising, under which each resized image is passed through the de-noising filter to remove some artifacts and noise from the input image. In every CT image, there is some important patients' information which is not useful for the desired task and using or sharing of such information is also against the ethical laws. So, this information is removed before using the images. At the end of this step, input images are in identical size, free from noise and patient's information (like his/her name, age, sex, date of scanning, time etc). So, the complete dataset is ready to use and passed to sample bifurcation.

The next step is bifurcation of input images into training and testing samples. In the sample bifurcation step ideally, the whole sample is dissected into three different sets called training, validation and testing set. The input dataset is divided into training, validation and testing sample sets in the ratio of 65:10:25. Therefore, the total number of training samples is 480, validation sample is 80 and remaining 186 samples are used as testing set. Among 480 training samples, 240 samples belong to Class 1 and the remaining 240 samples belong to Class 2 category. In the validation set, 40 samples are taken from both categories. For 186 testing samples, 69 samples belong to Class 1 and 117 samples belong to Class 2 case. The brief description of dataset bifurcation is given in **Table 2**.

Table 2 Data Distribution

Category	Total cases	Training set	Testing set	Validation set
Class 1	349	240	69	40
Class 2	397	240	117	40
Total:	**746**	**480**	**186**	**80**

After the training and testing set creation, normalization is performed. The major benefit of normalization is scaling and centering the data in the range of 0 and 1. It also improves the performance of the system and reduces the computation time. The normalized training and testing set is used for classification model building.

3.2.2 Model Building Section

The proposed model consists of two identity blocks named as IB-1 and IB-2 [47]. Each IB-X where, X= {1, 2} block consists of two paths one is called main path and other is called shortcut path. The structure of IB-1 and IB-2 are shown in **Fig. 5**.

The main path of IB-1 consists of three CONV_2D layers, three normalization layers and two non-linear activation functions 'ReLu'. Initially, X_{in} is passed through the main path and the output of main path is lastly added with original X_{in} using shortcut path and passed to the 'ReLu' for better performance. The IB-2 is similar to the IB-1 except the

shortcut path. This shortcut path is composed of CONV_2D and normalization layers. After that X_{out} is obtained using addition of main path output and shortcut path output. The mathematical expression of IB-1 and IB-2 output is given in Eq. (1) and Eq. (2).

$$X_{out} = F(X_{in}) + X_{in} \tag{1}$$

$$X_{out} = F(X_{in}) + X_{in}^{'} \tag{2}$$

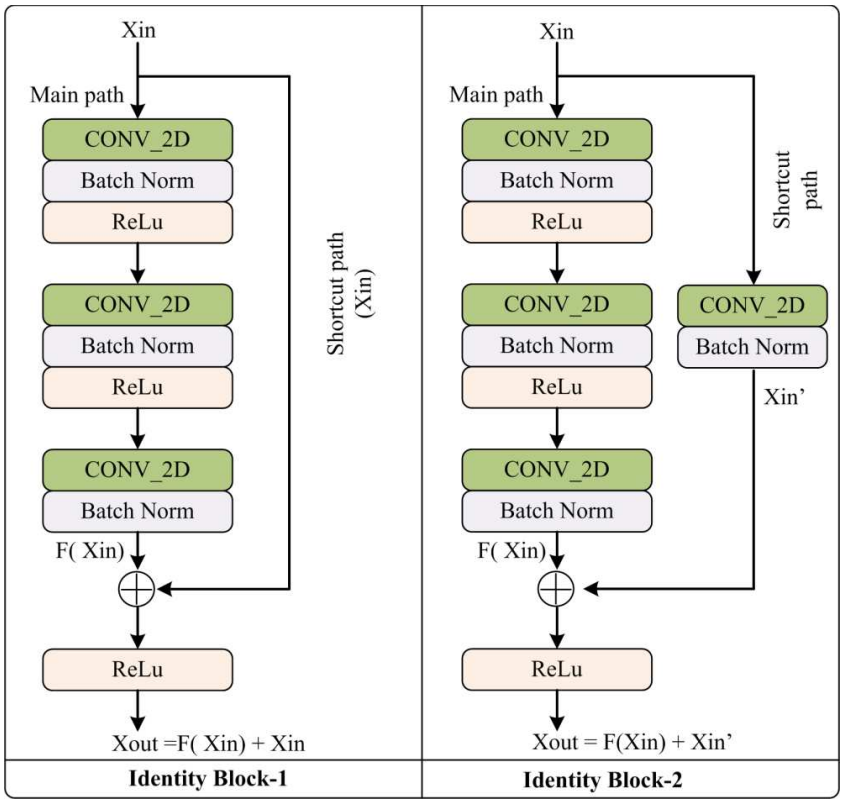

Fig. 5. Architecture of Identity Block

From the **Fig. 5**, it is observed that the main path of IB-1 and IB-2 has three layers. The first layer CONV_2D uses the F1 type filter of size [1 × 1] and stride of size [1 × 1] with valid padding. At second layerCONV_2D uses F2 type filter and at layer three CONV_2D uses F3 type filter of size [1 × 1] and stride of size [1 × 1] with valid padding. For each layer 0 is used as the seed value for the random initialization. In case of IB-2, the shortcut path consists of CONV_2D and batch normalization layer. In this CONV_2D uses F3 type filter of size [1 × 1] and stride of size [1 × 1] with valid padding.

The proposed deep neural network model is comprised of stack of layers and information flow between layers for the discrimination of infectious and non-infectious cases is shown in Fig. 6.

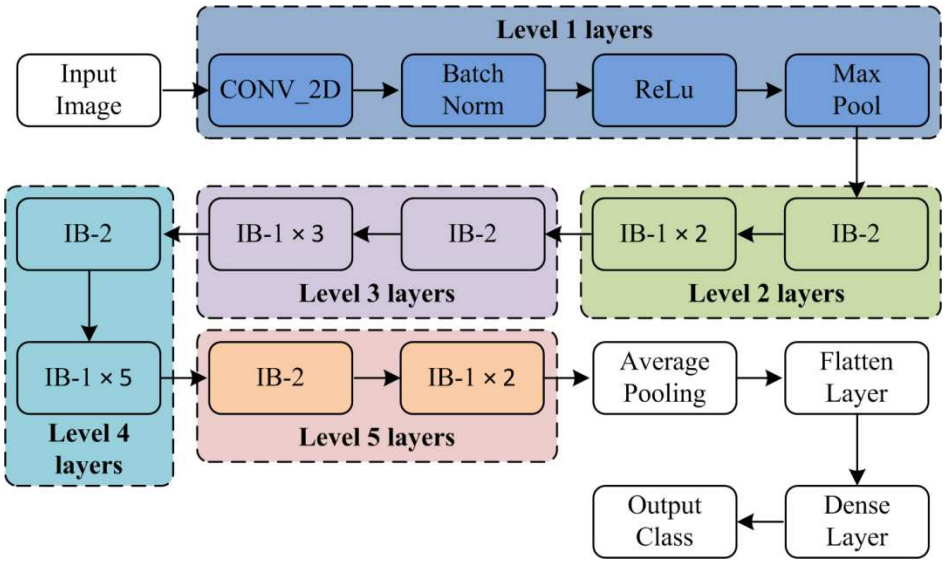

Fig. 6. Layer Wise Data Flow in Designed Model

The detailed description and architecture of the implemented model is given is **Fig. 7**.

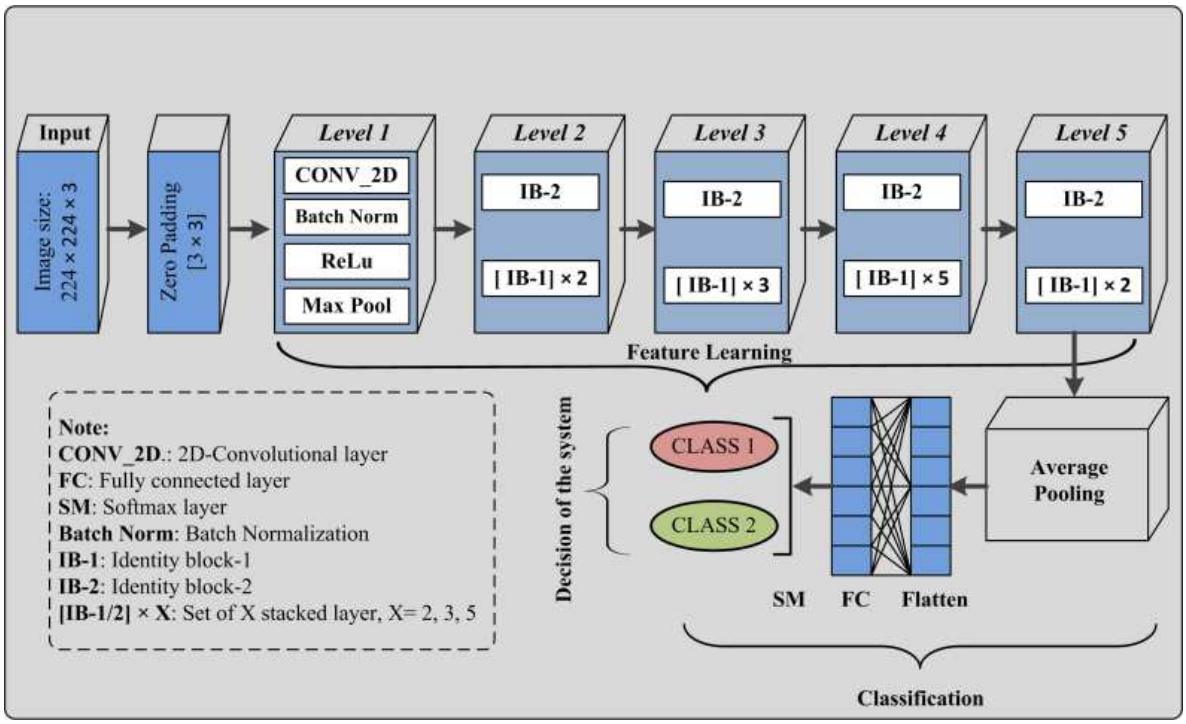

Fig. 7. Proposed Model: Computer Assisted Model for Analysis and Characterization of COVID19using CT Chest Images and Deep Neural Network

Initially, the input image is padded with zero padding of size [3 × 3], and then convolutional operation is performed using filter size [7 × 7] of 64 kernels with stride of [2 × 2]. The sequence of operation is followed by batch normalization, a non-linear activation function ReLu and max pooling. At this level pooling uses a window of size [3

× 3] with stride of [2 × 2] and at level 2, IB-2 uses three layered stack filters of size [64 × 64 × 256] with stride of [1 × 1]. The resultant of the operations is passed to two sets of IB-1 having three identical sets of filters with size [64 × 64 × 256]. At the next level of model, IB-2 is comprised of three sets of identical filters with size [128 × 128 × 512] with stride of [2 × 2]. After that three sets of IB-1 are used with three different sets of filters with size [128 × 128 × 512]. At level 4, three similar sets of filters with size [256 × 256 × 1024] are used with stride of [2 × 2]. This set is followed by five blocks of IB-1 using three sets of filters with size [256 × 256 × 1024]. At the next level of the proposed model, IB-2 uses three sets of filters with size [512 × 512 × 2048], and then the output of IB-2 is passed to the two identical blocks of IB-1 using three sets of filters with size [512 × 512 × 2048]. After that average pooling of windows size [2 × 2] is applied and then pooled features are passed to the flatten layer. The computed features are passed to a dense layer having 'softmax' function as an activation layer. Finally, according to 'softmax' layer output, decision takes place.

Optimized gradient descent

In past studies, it has been found that Optimized Gradient Descent or Stochastic Gradient Descent (SGD) is frequently used for DL model training and attain the promising result [48]. SGD is an optimization technique which is mathematically defined as given expression in Eq. 3 for training sample X_{in} with label Y_{in}.

$$\theta = \theta - \eta \nabla_{\theta} j(\theta, X_{in}^{(i)}, Y_{in}^{(i)}) \tag{3}$$

The algorithm used for SGD training is described in Algorithm 1.

Algorithm 1: SGD Training Algorithm

```
START
Initialize(nn)
No_of_batch = total_image/size_batch
epoch_number: n
  for epoch_number 1:n
    {
     do {
        for size_batch 1: m
        {
          do {
              in= random samples of images are selected according to batch size
                        [Xin, Yin] = pre-process(in)
                        Zin = feed-forward(nn, Xin)
                        entropy_loss = entopy_loss(Zin, Yin]
                        gradient_back = feed-backward(entropy_loss)
                        update(nn, gradient_back)
            }
        } end for
       }
  } end for
STOP
```

The mathematical expression of entropy loss is defined as Eq. 4.

$$entropy\_loss = -\{y\log(p) + (1-y)\log(1-p)\} \quad (4)$$

3.2.3 Decision making section

In the proposed model, level 1 to level 5 are used for feature learning purpose. After feature learning, classification is performed using the average pooling layer, flatten layer, FC layer and soft-max layer. In the classification section, the instance of testing set is passed to the validated model and then obtained class label is considered as the decision of the proposed system for the particular input test sample. In the same manner, the whole test sample is passed to the validated model that assigned a label to each input sample. The performance of the model is evaluated using performance metrics, which is described in the next section.

3.3 Performance metrics

The performance of proposed work is evaluated with the help of classification accuracy, sensitivity, specificity, precision and F1score [49-50]. All parameters are obtained by the help of confusion matrix. The structure of confusion matrix (CM) is shown in **Fig. 8**. The mathematical expression of used parameters is given in Eq. 5, Eq. 6, Eq. 7, Eq. 8, and Eq. 9.

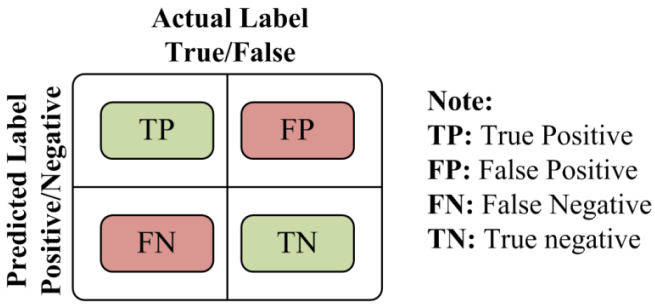

Fig. 8. structure of confusion matrix

$$Class\_Acc(\%) = \frac{TP+TN}{TP+TN+FP+FN} \times 100 \quad (5)$$

$$Sensitivity(\%) = \frac{TP}{TP+FN} \times 100 \quad (6)$$

$$Specificity(\%) = \frac{TN}{TN+FP} \times 100 \quad (7)$$

$$Precision(\%) = \frac{TP}{TP+FP} \times 100 \quad (8)$$

$$F1score = 2 \times \frac{Precision * Sensitivity}{Precision + Sensitivity} \quad (9)$$

4. EXPERIMENT AND RESULT

In this paper, extensive work has been carried for the analysis and characterization of COVID19 using CT chest images. To achieve desired outcome, deep neural network with optimized gradient descent has been used. The environmental setup for experiment execution and obtained results are discussed in next section.

4.1 Experimental Setup

The entire experimentation is performed using HP Z4 G4 workstation. This system has the below mentioned specification: Intel Xeon W-2014 CPU @ 3.2 GHz, 2TB SATA HDD and 256 GB SSD, 4GB NVIDIA Quadro P1000 and 64 GB RAM. All the images and ROIs are stored in this system and the experiments are performed using the Python environment.

4.2 Experiment and Result

In this experiment an image dataset of 746 CT scan is used. A set of 746 images consists of 349 cases of Class 1 and 397 cases of Class 2 category. Among 746 cases, 480 samples are used as a training set, 80 samples are used as validation sets and the remaining 186 samples are used as a testing set. Initially, the designed model M1 is trained using training set for 50 epoch and the trained model is validated using validation set. After that testing set is passed to the model and obtained result is given in **Table 3**.

Table 3. Obtained Results for Proposed Work

	CM		Class_Acc (%)	Sen(%)	Spe (%)	Prec (%)	F1score (%)
	C 1	C 2					
C 1	67	2	98.4	98.5	98.3	97.1	97.8
C 2	1	116					

Note: C1: Class 1; C2: Class 2; CM: Confusion Matrix; Class_Acc: Classification Accuracy; Sen: Sensitivity; Spe: Specificity; Prec: Precision.

The performance of experimentation done on the designed model is calculated in the form of classification accuracy (Class_Acc), specificity (Spe), sensitivity (Sen), precision (Prec) and F1score using previously mentioned equations. The obtained value of each parameter is shown in **Fig. 9**.

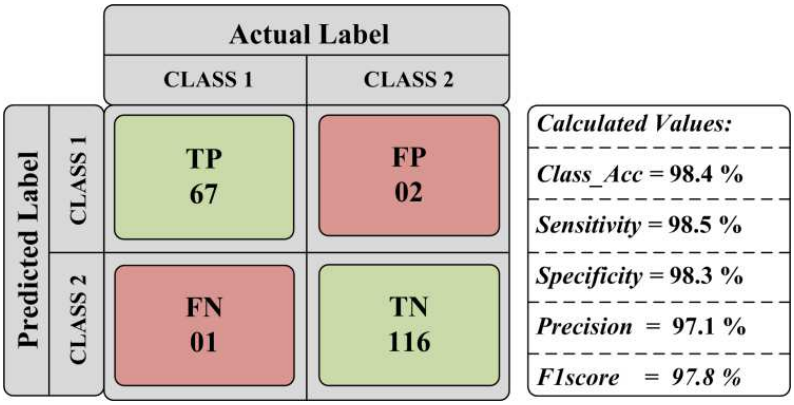

Fig. 9. Obtained parametric value

The performance of the proposed model through the training phase is measured in the form of training accuracy and loss. While the performance of the trained model during the validation phase is measured in the form of validation accuracy and validation loss. During the training and validation, the performance of the proposed model is outstanding, and the achieved training accuracy is 97.7 % and training loss is 0.52. The validation accuracy of the model is achieved as 98.4 % and validation loss is 0.502. The curve between training and validation loss is shown in **Fig. 10** and comparative analysis of training accuracy and validation accuracy is shown in **Fig. 11**.

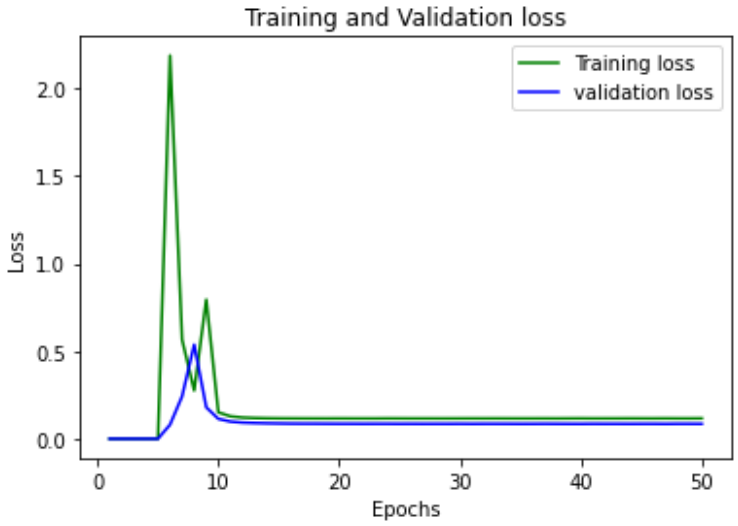

Fig. 10. Performance Curve for Training vs. Validation Loss

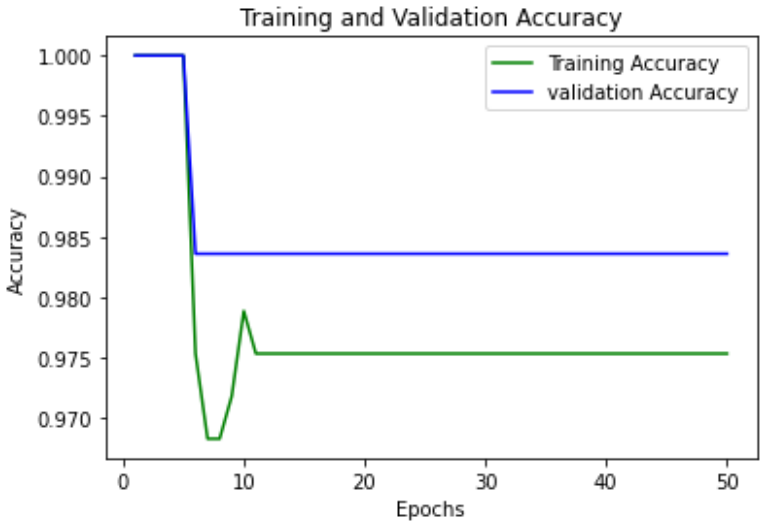

Fig. 11. Performance Curve for Training vs. Validation Accuracy

4.3 Result Analysis

The outcome of the proposed model is further analyzed by two different approaches: quantitative and statistical analysis. Under quantitative analysis, accuracy, sensitivity, specificity, precision and F1score is computed, and Cohen's kappa analysis is used for statistical analysis.

4.3.1 Quantitative Analysis

After the regressive work, the obtained results of 186 testing samples are reported in **Table 2** and observed that the achieved classification accuracy is 98.4%. The proposed model yields 98.5% of sensitivity, 98.3% of specificity, 97.1% of precision and 97.8% of F1score as shown in **Fig. 12**.

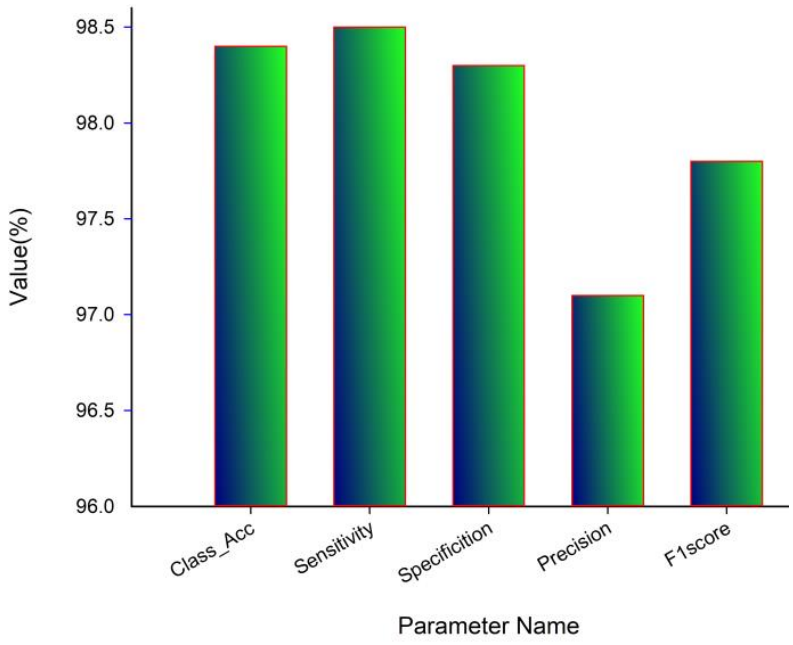

Fig. 12. Quantitative Analysis of Proposed Work

The classification accuracy of proposed system 98.4% (183/186) shows that the 183 samples are correctly classified from 186 samples. From 183 correctly classified samples, 67 samples of positive case (Class 1) out of 69 cases are detected while 116 samples of negative case (Class 2) out of 117 samples are correctly detected. Out of 69 Class 1 cases, 2 cases are predicted as negative and out of 117 Class 2 samples, 1 case is predicted as Class 1. Therefore, the total 3 cases are misclassified out of 186 cases. The misclassification accuracy of the system is obtained as 1.6 % (3/186). From 3 misclassified samples, two samples belong to Class 1 category and one sample belongs to the Class 2 category.

The performance of the proposed system for individual class classification is obtained as 97.1% (67/69) for positive cases (Class 1) and 99.1 % (116/117) for negative cases (Class 2). For 69 test samples of class 1, 67 samples are correctly classified and 116 out of 117 cases of Class 2 are correctly detected.

4.3.2 Statistical Analysis

The statistical analysis is performed with Cohen's kappa coefficient [51]. It shows the significance or reliability of the proposed work. The kappa coefficient τ is calculated with the help of given Eq. 10.

$$\tau = \frac{p_0 - p_e}{1 - p_e} \tag{10}$$

Where τ is kappa value, P_0 is the probability of observed agreement and p_e is the probability of hypothetical agreement. With the help of confusion matrix, P_0 and P_e are computed as Eq. 11 and Eq. 12, respectively:

$$P_0 = \frac{TP + TN}{TP + TN + FP + FN} \tag{11}$$

and

$$p_e = p_{Class1} + p_{Class2} \tag{12}$$

Where, $P_{Class\ 1}$ and $P_{Class\ 2}$ are computed as given expression i. e. Eq. 13.

$$\begin{aligned} P_{Class1} &= \frac{TP + FP}{TP + FP + TN + FN} * \frac{TP + FN}{TP + FP + TN + FN} \\ P_{class2} &= \frac{FN + TN}{TP + FP + TN + FN} * \frac{FP + TN}{TP + FP + TN + FN} \end{aligned} \tag{13}$$

With the help of confusion matrix given in Table 2, the value of TP is 67, the value of FP is 2, the value of FN is 1 and the value of TN is 116. By using these values P_0 and P_e is computed and the obtained value of P_0 and P_e is helpful in computation of kappa value. So, the value of P_0 and P_e is computed as:

$$P_0 = \frac{67 + 116}{67 + 2 + 1 + 116} = \frac{183}{186} = 0.984$$

Similarly, the value of remaining term is obtained as P_e=0.534 , P_0-P_e=0.449 , 1-P_e=0.465 , τ = 0.965 and kappa error = 0.0199. As per the obtained value of kappa coefficient, the reliability of the proposed model is high.

4.4 Comparative Analysis

The present work is directly compared with the study performed by J. Zhao et al., 2020 [46] because both are using the same set of images. The same work is also compared with the study performed by different authors [43, 45, 46, 52]. The comparative analysis is presented in **Table 4** and **Fig. 13**.

Table 4 Comparative Analysis between Proposed Works with State-of-the-art

Author(s), Year	**Class_Acc. (%)**	**Sens. (%)**	**Spec. (%)**	**Prec. (%)**	**F1score (%)**
L. Li et. al., 2020. [43]	96 %	90. %	96%	--	--
C. Butt et. al., 2020, [45]	--	86.7	--	81.3	83.9
J. Zhao et al., 2020 [46]	84.7	76.2	--	97.0	85.3
HX. Bai et al., 2020, [52]	96	95	96	90.	--
Proposed	98.4	98.5	98.3	97.1	97.8

From **Table 4**, it has been clearly seen that the proposed work performs better in every aspect with respect to studies [43, 45, 46, 52]. The classification accuracy of the proposed work is superior among previously published work, which makes the system more stable. In the same manner, proposed work yields better sensitivity value, specificity value, precision and F1score. Thus, it can be concluded that the proposed work is better than the previously published work.

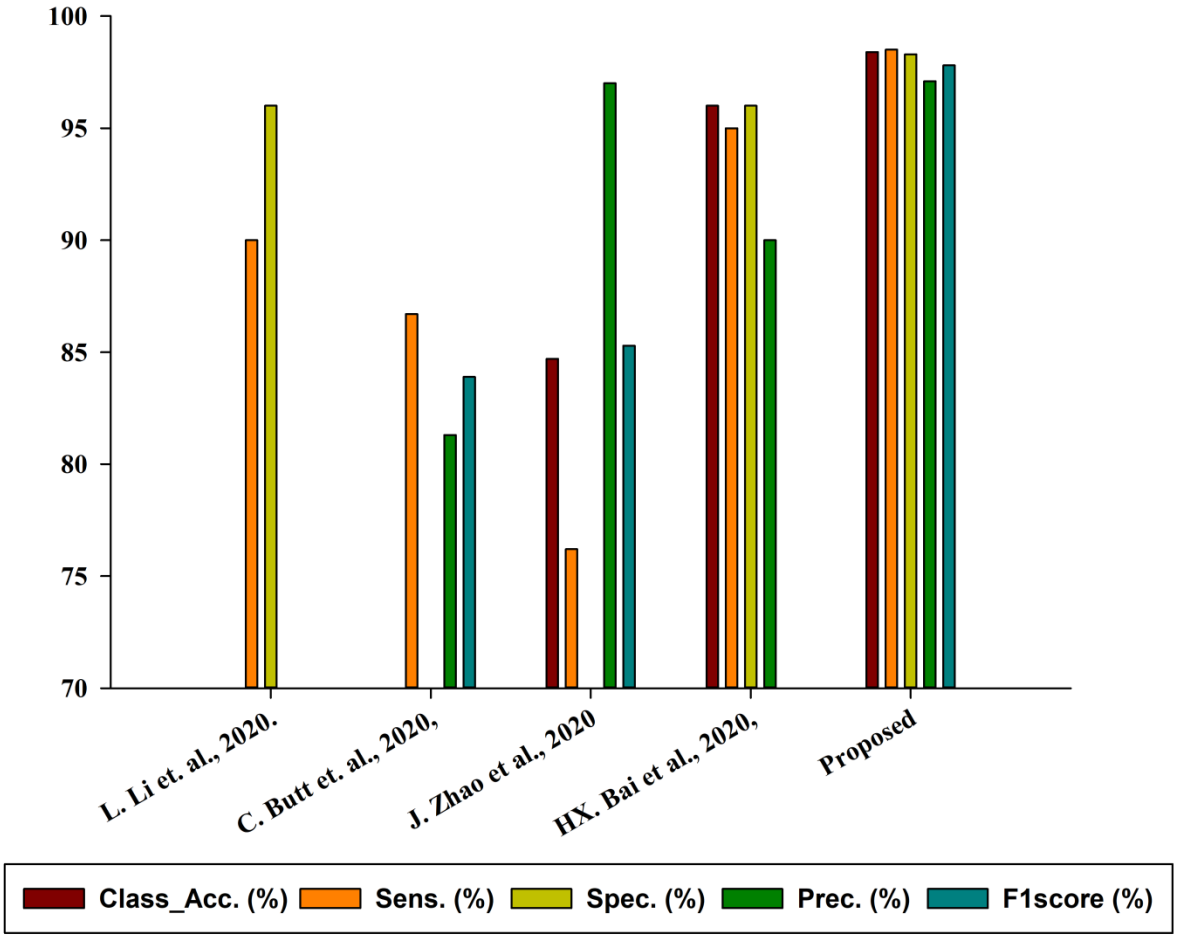

Fig. 13. Comparative Analysis between Proposed Works with State-of-the-art.

5. CONCLUSION

The majority of the deaths due to COVID19 are observed when it causes pneumonia, which itself is a huge threat for lives of general public due to its rapidly growing and fatal nature as well as its high incidence. Therefore, initial and accurate diagnosis of the ailment using every available and feasible technology is must for avoiding the grim consequences of the pandemic. The present work focused on one of such technology i.e., chest CT scans, which proved to prompt feasible and highly sensitive for such task. The proposed AI-based approach for the detection of COVID19 shows promising results with the high accuracy of 98.4 %, precision of 97.1 %, sensitivity of 98.5 %, the specificity of 98.3 % and F1 score of 97.8 %. The database used about 746 chests scanned CT images containing both infected subjects with COVID19 and normal subjects too. The results obtained by utilizing various COVID19 features of CT imaging shows that artificial intelligence-based techniques can be utilized for diagnosing the potential patients more efficiently and reliably.

The logical conclusion seems to indicate that it is hard to overcome the present COVID19 pandemic due to the highly contagious and mutating nature of its corresponding virus i.e., SARS-CoV2 but it can be prevented using the lessons

learned about the preventive measures from other pandemics like MERS-CoV or SARS-CoV. This preventive measure includes using facial covers or masks, personal hygiene, maintaining social distancing and proper isolation or quarantine for potential patients of the disease. Moreover, the early diagnosis of such potential patients using whichever technique available in the area as resources are always overloaded during the pandemic. Such measures are crucial until every person in the world is completely vaccinated, as due to high mutating nature of the virus, the possibility of virus mutating to vaccine resistant variant cannot be denied. Finally, the future scope would focus on developing a robust system for AI-based diagnosis, monitoring and data collection to enable the future generation to have ample resources to deal with any pandemic.

DECLARATION

N/A

FUNDING

N/A

CONFLICTS OF INTEREST/COMPETING INTERESTS

There is no conflict of the interest from authors side.

AVAILABILITY OF DATA AND MATERIAL

https://github.com/UCSD-AI4H/COVID-CT

CODE AVAILABILITY

N/A

REFERENCE

1 World Health Organization, Novel Coronavirus(2019-nCoV)Situation Report-44. 2020. https://www.who.int/docs/default-source/coronaviruse/situation-reports/20200508covid-19-sitrep-109.pdf?sfvrsn=68f2c632_6 Accessed 19th March 2020.

2 World Health Organization, Novel Coronavirus(2019-nCoV)Situation Report-109. 2020. https://www.who.int/docs/default-source/coronaviruse/situation-reports/20200508covid-19-sitrep-109.pdf?sfvrsn=68f2c632_6 Accessed 9th May 2020.

3 Worldometer Coronavirus. https://www.worldmeters.info/coronavirus/countries where-coronavirus-has-spread/. Accessed 18th May 2021.

4 Mousavizadeh, L. and Ghasemi, S., 2020. Genotype and phenotype of COVID-19: Their roles in pathogenesis. *Journal of Microbiology, Immunology and Infection*.

5 Cascella, M., Rajnik, M., Cuomo, A., Dulebohn, S.C. and Di Napoli, R., 2020. Features, evaluation and treatment coronavirus (COVID-19). In *Statpearls [internet]*. StatPearls Publishing.

6 Shi, F., Wang, J., Shi, J., Wu, Z., Wang, Q., Tang, Z., He, K., Shi, Y. and Shen, D., 2020. Review of artificial intelligence techniques in imaging data acquisition, segmentation and diagnosis for covid-19. *IEEE Reviews in Biomedical Engineering*.

WHO. Middle East respiratory syndrome coronavirus (MERS-CoV). November, 2019. http://www.who.int/emergencies/mers-cov/en/ (accessed March 15, 2020).

World Health Organization. International clinical trials registry platform. 2020. https://apps.who.int/trialsearch/default.aspx. (Accessed 13th May 2020)

Wang, D., Hu, B., Hu, C., Zhu, F., Liu, X., Zhang, J., Wang, B., Xiang, H., Cheng, Z., Xiong, Y. and Zhao, Y., 2020. Clinical characteristics of 138 hospitalized patients with 2019 novel coronavirus–infected pneumonia in Wuhan, China. Jama, 323(11), pp.1061-1069

Chen, N., Zhou, M., Dong, X., Qu, J., Gong, F., Han, Y., Qiu, Y., Wang, J., Liu, Y., Wei, Y. and Yu, T., 2020. Epidemiological and clinical characteristics of 99 cases of 2019 novel coronavirus pneumonia in Wuhan, China: a descriptive study. *The Lancet*, *395*(10223), pp.507-513.

Li, Q., Guan, X., Wu, P., Wang, X., Zhou, L., Tong, Y., Ren, R., Leung, K.S., Lau, E.H., Wong, J.Y. and Xing, X., 2020. Early transmission dynamics in Wuhan, China, of novel coronavirus–infected pneumonia. *New England Journal of Medicine*.

Chu, D.K., Pan, Y., Cheng, S.M., Hui, K.P., Krishnan, P., Liu, Y., Ng, D.Y., Wan, C.K., Yang, P., Wang, Q. and Peiris, M., 2020. Molecular diagnosis of a novel coronavirus (2019-nCoV) causing an outbreak of pneumonia. *Clinical chemistry*, *66*(4), pp.549-555

Li, L., Zhang, Q., Wang, X., Zhang, J., Wang, T., Gao, T.L., Duan, W., Tsoi, K.K.F. and Wang, F.Y., 2020. Characterizing the propagation of situational information in social media during COVID-19 epidemic: A case study on weibo. *IEEE Transactions on Computational Social Systems*, *7*(2), pp.556-562.

Zhang N, Wang L, Deng X, Liang R, Su M, He C, et al. Recent advances in the detection of respiratory virus infection in humans. J Med Virol. 2020

Chung, M., Bernheim, A., Mei, X., Zhang, N., Huang, M., Zeng, X., Cui, J., Xu, W., Yang, Y., Fayad, Z.A. and Jacobi, A., 2020. CT imaging features of 2019 novel coronavirus (2019-nCoV). *Radiology*, *295*(1), pp.202-207

Gomez, P., Semmler, M., Schützenberger, A., Bohr, C. and Döllinger, M., 2019. Low-light image enhancement of high-speed endoscopic videos using a convolutional neural network. *Medical & biological engineering & computing*, *57*(7), pp.1451-1463

Choe, J., Lee, S.M., Do, K.H., Lee, G., Lee, J.G., Lee, S.M. and Seo, J.B., 2019. Deep Learning–based Image Conversion of CT Reconstruction Kernels Improves Radiomics Reproducibility for Pulmonary Nodules or Masses. *Radiology*, *292*(2), pp.365-373

Kermany, D.S., Goldbaum, M., Cai, W., Valentim, C.C., Liang, H., Baxter, S.L., McKeown, A., Yang, G., Wu, X., Yan, F. and Dong, J., 2018. Identifying medical diagnoses and treatable diseases by image-based deep learning. *Cell*, *172*(5), pp.1122-1131

Negassi, M., Suarez-Ibarrola, R., Hein, S., Miernik, A. and Reiterer, A., 2020. Application of artificial neural networks for automated analysis of cystoscopic images: a review of the current status and future prospects. *World Journal of Urology*, pp.1-10.

Wang, P., Xiao, X., Brown, J.R.G., Berzin, T.M., Tu, M., Xiong, F., Hu, X., Liu, P., Song, Y., Zhang, D. and Yang, X., 2018. Development and validation of a deep-learning algorithm for the detection of polyps during colonoscopy. *Nature biomedical engineering*, *2*(10), pp.741-748

Koo, H.J., Lim, S., Choe, J., Choi, S.H., Sung, H. and Do, K.H., 2018. Radiographic and CT features of viral pneumonia. *Radiographics*, *38*(3), pp.719-739

Wang, D., Hu, B., Hu, C., Zhu, F., Liu, X., Zhang, J., Wang, B., Xiang, H., Cheng, Z., Xiong, Y. and Zhao, Y., 2020. Clinical characteristics of 138 hospitalized patients with 2019 novel coronavirus–infected pneumonia in Wuhan, China. *Jama*, *323*(11), pp.1061-1069.

Wang, S., Kang, B., Ma, J., Zeng, X., Xiao, M., Guo, J., Cai, M., Yang, J., Li, Y., Meng, X. and Xu, B., 2020. A deep learning algorithm using CT images to screen for Corona Virus Disease (COVID-19). *MedRxiv*.

Chua, F., Armstrong-James, D., Desai, S.R., Barnett, J., Kouranos, V., Kon, O.M., José, R., Vancheeswaran, R., Loebinger, M.R., Wong, J. and Cutino-Moguel, M.T., 2020. The role of CT in case ascertainment and management of COVID-19 pneumonia in the UK: insights from high-incidence regions. *The Lancet Respiratory Medicine*.

Ai T, Yang Z, Hou H, et al. Correlation of chest CT and RT-PCR testing in coronavirus disease 2019 (COVID-19) in China: a report of 1014 cases. Radiology 2020; published online Feb 26. DOI:10·1148/radiol.2020200642

Xie X, Zhong Z, Zhao W, Zheng C, Wang F, Liu J. Chest CT for typical 2019-nCoV pneumonia: relationship to negative RT-PCR testing. Radiology 2020; published Feb 12. DOI:10·1148/radiol.2020200343

Bernheim A, Mei X, Huang M, et al. Chest CT findings in coronavirus disease-19 (COVID-19): relationship to duration of infection. Radiology 2020; published Feb 20. DOI:10·1148/radiol.2020200463.

Chung M, Bernheim A, Mei X, et al. CT imaging features of 2019 novel coronavirus (2019-nCoV). Radiology 2020; published online Feb 4. DOI:10·1148/radiol.2020200230.

Pan F, Ye T, Sun P, et al. Time course of lung changes on chest CT during recovery from 2019 novel coronavirus (COVID-19) pneumonia. Radiology 2020; published online Feb 13. DOI:10·1148/radiol.2020200370

Fang Y, Zhang H, Xie J, et al. Sensitivity of chest CT for COVID-19: comparison to RT-PCR. Radiology 2020; published Feb 19. DOI:0·1148/ radiol.2020200432.

Bai HX, Hsieh B, Xiong Z, et al. Performance of radiologists in differentiating COVID-19 from viral pneumonia on chest CT. Radiology 2020; published online March 10. DOI:10.1148/radiol.2020200823.

Tabatabaei, S.M.H., Talari, H., Moghaddas, F. and Rajebi, H., 2020. Computed Tomographic Features and Short-term Prognosis of Coronavirus Disease 2019 (COVID-19) Pneumonia: A Single-Center Study from Kashan, Iran. *Radiology: Cardiothoracic Imaging*, *2*(2), p.e200130.

Centers for Disease Control and Progression. Corona virus 2019 disease (COVID-19). https://www.cdc.gov/coronavirus/2019-ncov/cases-in-us.html

Ng, M.Y., Lee, E.Y., Yang, J., Yang, F., Li, X., Wang, H., Lui, M.M.S., Lo, C.S.Y., Leung, B., Khong, P.L. and Hui, C.K.M., 2020. Imaging profile of the COVID-19 infection: radiologic findings and literature review. *Radiology: Cardiothoracic Imaging*, *2*(1), p.e200034.

Zhao, W., Zhong, Z., Xie, X., Yu, Q. and Liu, J., 2020. Relation between chest CT findings and clinical conditions of coronavirus disease (COVID-19) pneumonia: a multicenter study. *American Journal of Roentgenology*, pp.1-6.

Pan, Y., Guan, H., Zhou, S., Wang, Y., Li, Q., Zhu, T., Hu, Q. and Xia, L., 2020. Initial CT findings and temporal changes in patients with the novel coronavirus pneumonia (2019-nCoV): a study of 63 patients in Wuhan, China. *European radiology*, pp.1-4.

Shi, H., Han, X., Jiang, N., Cao, Y., Alwalid, O., Gu, J., Fan, Y. and Zheng, C., 2020. Radiological findings from 81 patients with COVID-19 pneumonia in Wuhan, China: a descriptive study. *The Lancet Infectious Diseases*.

Guan, W.J., Ni, Z.Y., Hu, Y., Liang, W.H., Ou, C.Q., He, J.X., Liu, L., Shan, H., Lei, C.L., Hui, D.S. and Du, B., 2020. Clinical characteristics of coronavirus disease 2019 in China. *New England journal of medicine*, *382*(18), pp.1708-1720.

Inui, S., Fujikawa, A., Jitsu, M., Kunishima, N., Watanabe, S., Suzuki, Y., Umeda, S. and Uwabe, Y., 2020. Chest CT findings in cases from the cruise ship "Diamond Princess" with coronavirus disease 2019 (COVID-19). *Radiology: Cardiothoracic Imaging*, *2*(2), p.e200110.

Lee, E.Y., Ng, M.Y. and Khong, P.L., 2020. COVID-19 pneumonia: what has CT taught us?. *The Lancet Infectious Diseases*, *20*(4), pp.384-385.

Li, Y. and Xia, L., 2020. Coronavirus disease 2019 (COVID-19): role of chest CT in diagnosis and management. *American Journal of Roentgenology*, pp.1-7.

Xia, W., Shao, J., Guo, Y., Peng, X., Li, Z. and Hu, D., 2020. Clinical and CT features in pediatric patients with COVID-19 infection: Different points from adults. *Pediatric pulmonology*, *55*(5), pp.1169-1174.

Li, L., Qin, L., Xu, Z., Yin, Y., Wang, X., Kong, B., Bai, J., Lu, Y., Fang, Z., Song, Q. and Cao, K., 2020. Artificial intelligence distinguishes COVID-19 from community acquired pneumonia on chest CT. *Radiology*, p.200905.

Dadário, A.M.V., Paiva, J.P.Q., Chate, R.C., Machado, B.S. and Szarf, G., 2020. Regarding" Artificial Intelligence Distinguishes COVID-19 from Community Acquired Pneumonia on Chest CT". *Radiology*, p.201178.

Butt, C., Gill, J., Chun, D. and Babu, B.A., 2020. Deep learning system to screen coronavirus disease 2019 pneumonia. *Applied Intelligence*, p.1.

Zhao, J., Zhang, Y., He, X. and Xie, P., 2020. COVID-CT-Dataset: a CT scan dataset about COVID-19. *arXiv preprint arXiv:2003.13865*.

47 Deng, Li. "A tutorial survey of architectures, algorithms, and applications for deep learning." APSIPA Transactions on Signal and Information Processing 3 (2014).
48 Liu, Yaxi, Wei Huangfu, Haijun Zhang, and Keping Long. "An Efficient Stochastic Gradient Descent Algorithm to Maximize the Coverage of Cellular Networks." IEEE Transactions on Wireless Communications 18, no. 7 (2019): 3424-3436.
49 Kumar, Indrajeet, H. S. Bhadauria, Jitendra Virmani, and Shruti Thakur. "A classification framework for prediction of breast density using an ensemble of neural network classifiers." Biocybernetics and Biomedical Engineering 37, no. 1 (2017): 217-228.
50 Rawat, Jyoti, Annapurna Singh, H. S. Bhadauria, Jitendra Virmani, and J. S. Devgun. "Classification of acute lymphoblastic leukaemia using hybrid hierarchical classifiers." Multimedia Tools and Applications 76, no. 18 (2017): 19057-19085.
51 Viera, Anthony J., and Joanne M. Garrett. "Understanding interobserver agreement: the kappa statistic." Fam med 37, no. 5 (2005): 360-363.
52 Bai, Harrison X., Robin Wang, Zeng Xiong, Ben Hsieh, Ken Chang, Kasey Halsey, Thi My Linh Tran et al. "AI Augmentation of Radiologist Performance in Distinguishing COVID-19 from Pneumonia of Other Etiology on Chest CT." Radiology (2020): 201491.

Figures

Figure 1

Basic CT findings: (a) Ground glass opacities, (b) Consolidations and (c) Crazy paving patterns [46].

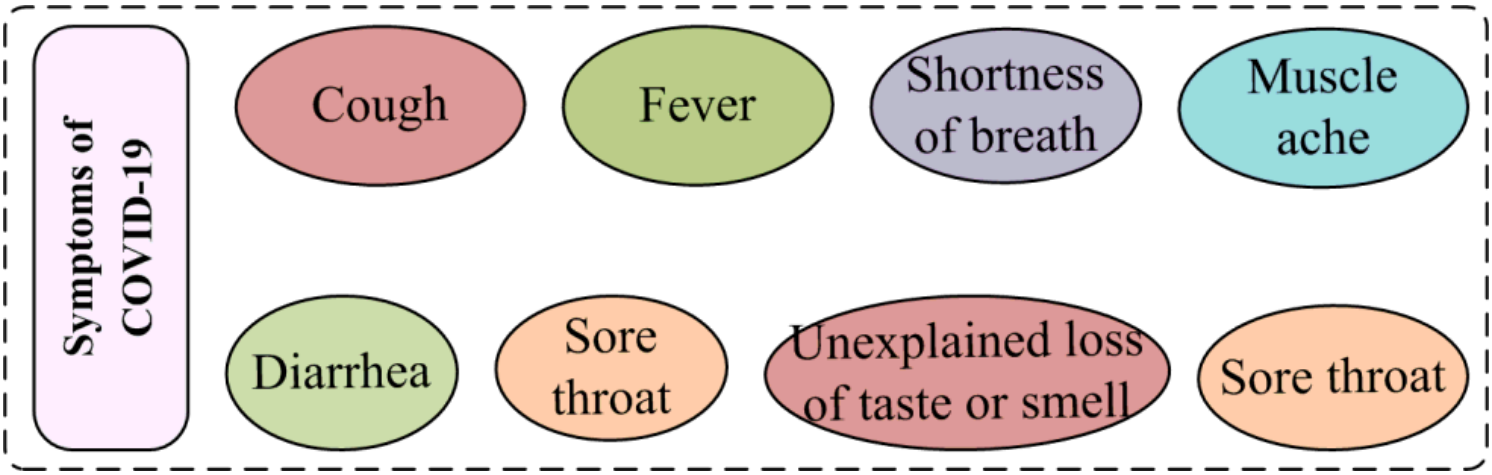

Figure 2

Major symptoms of the development of COVID-19 [1-2].

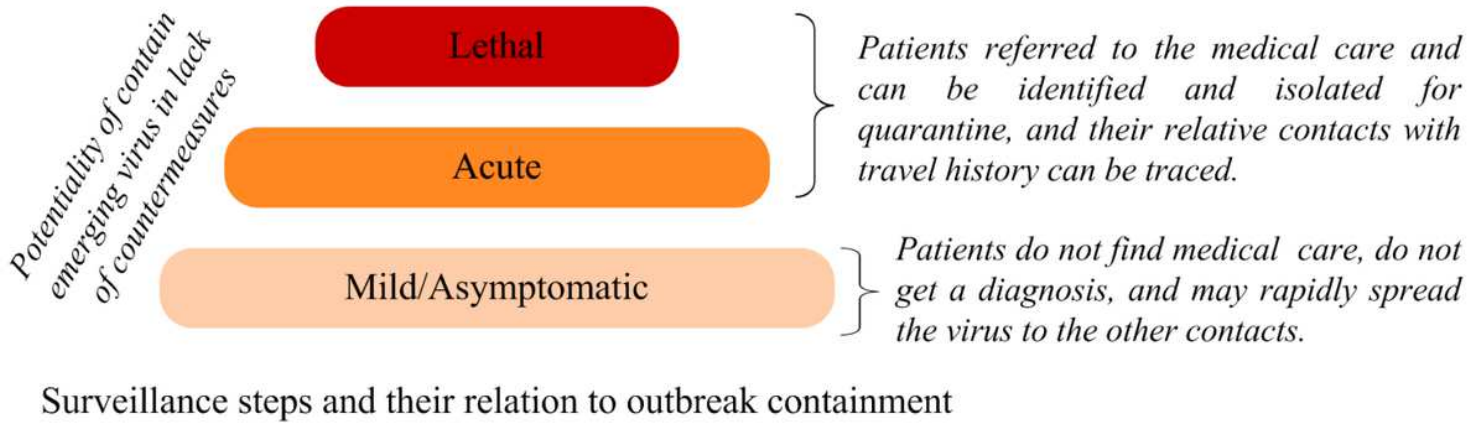

Figure 3

The major surveillance steps and their relation to COVID-19 containment [3].

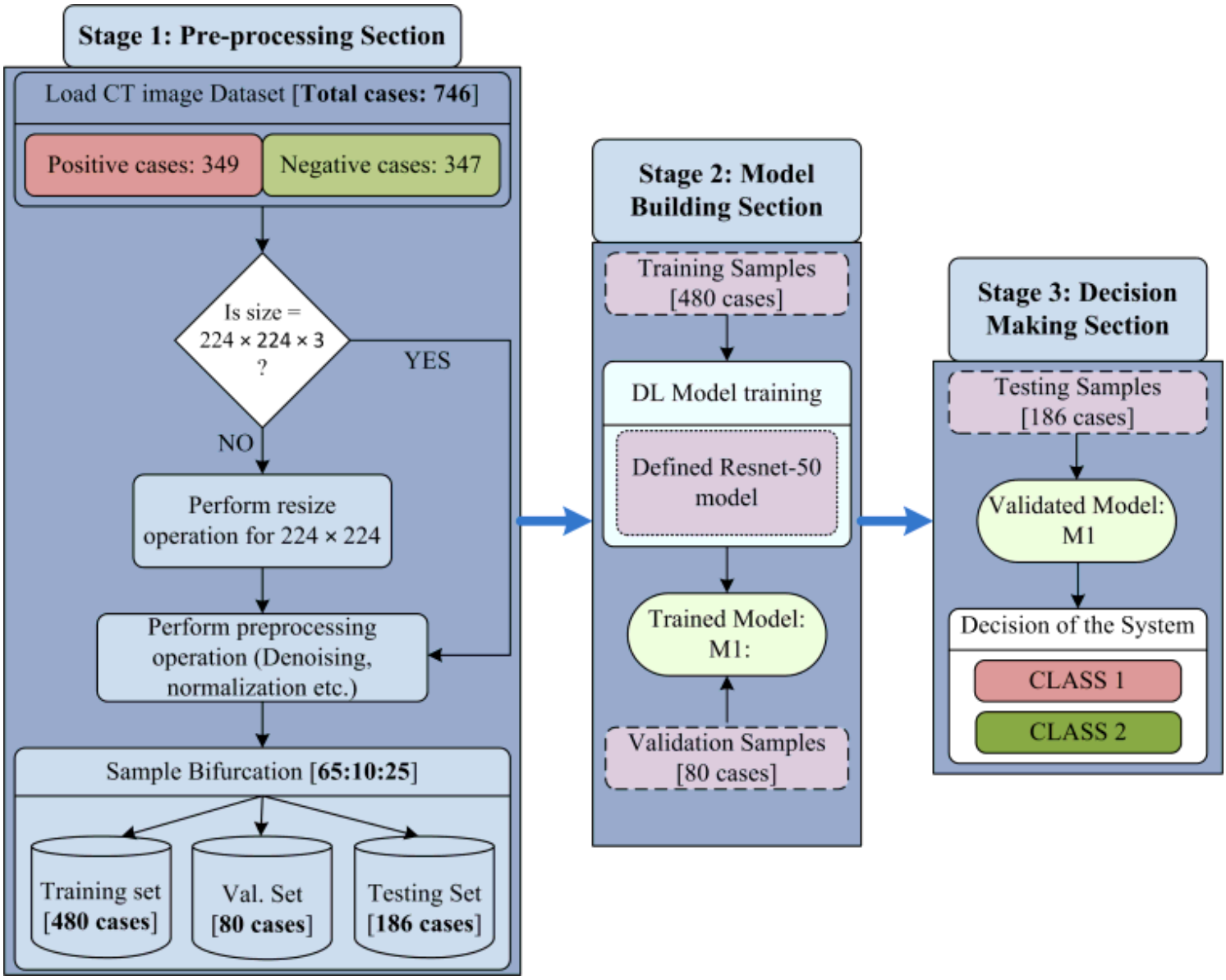

Figure 4

Experimental Workflow Diagram of Proposed Model

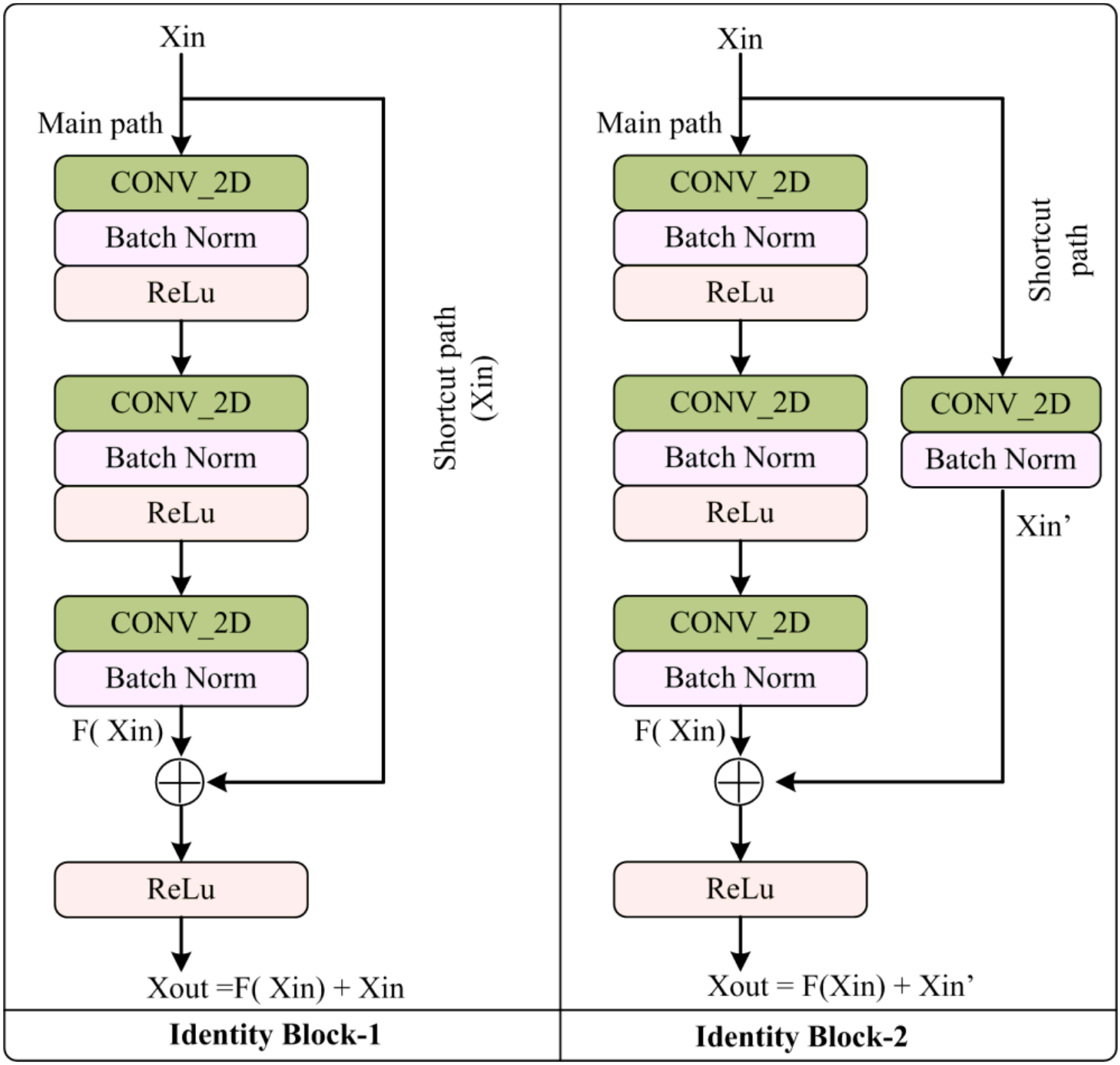

Figure 5

Architecture of Identity Block

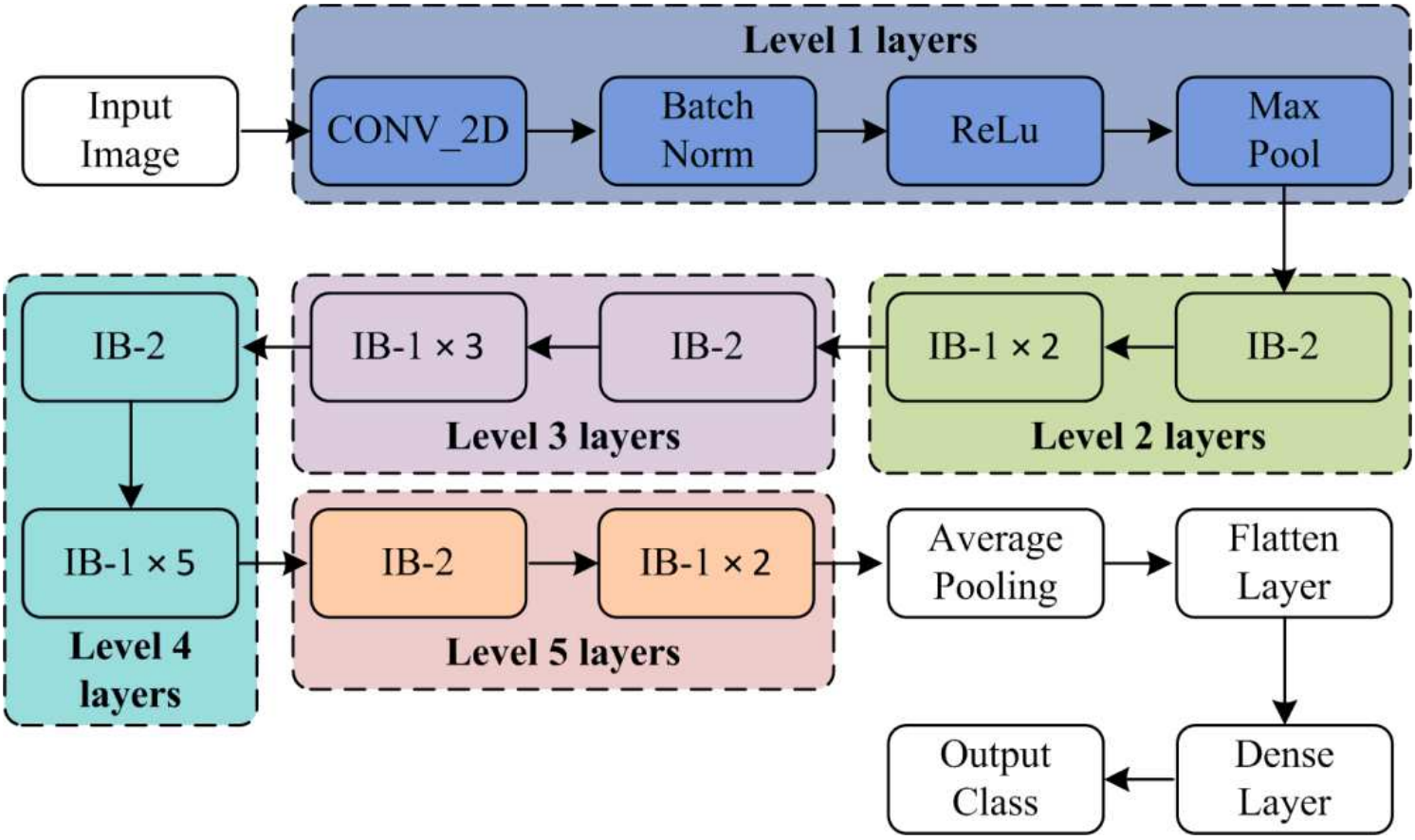

Figure 6

Layer Wise Data Flow in Designed Model

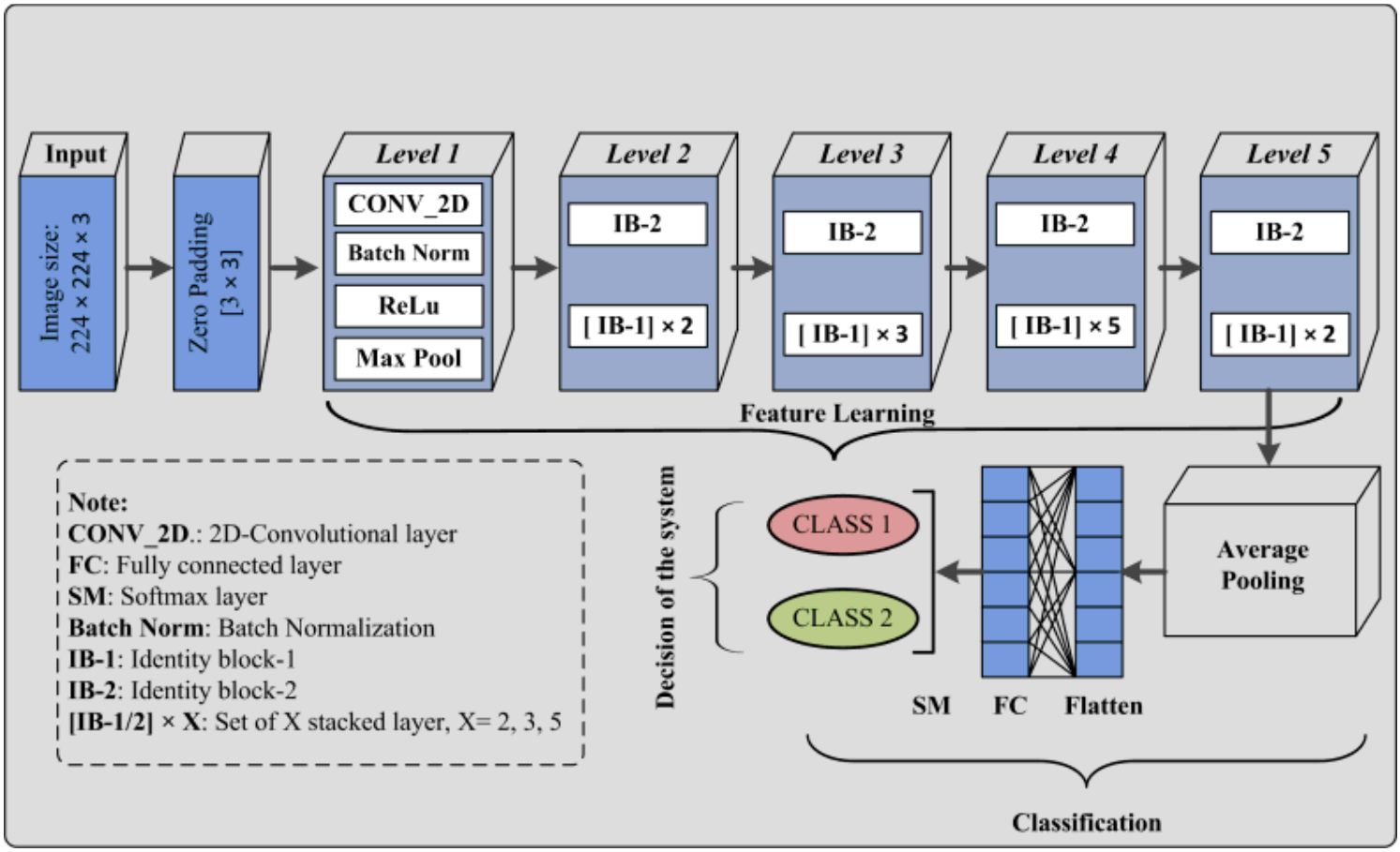

Figure 7

Proposed Model: Computer Assisted Model for Analysis and Characterization of COVID19using CT Chest Images and Deep Neural Network

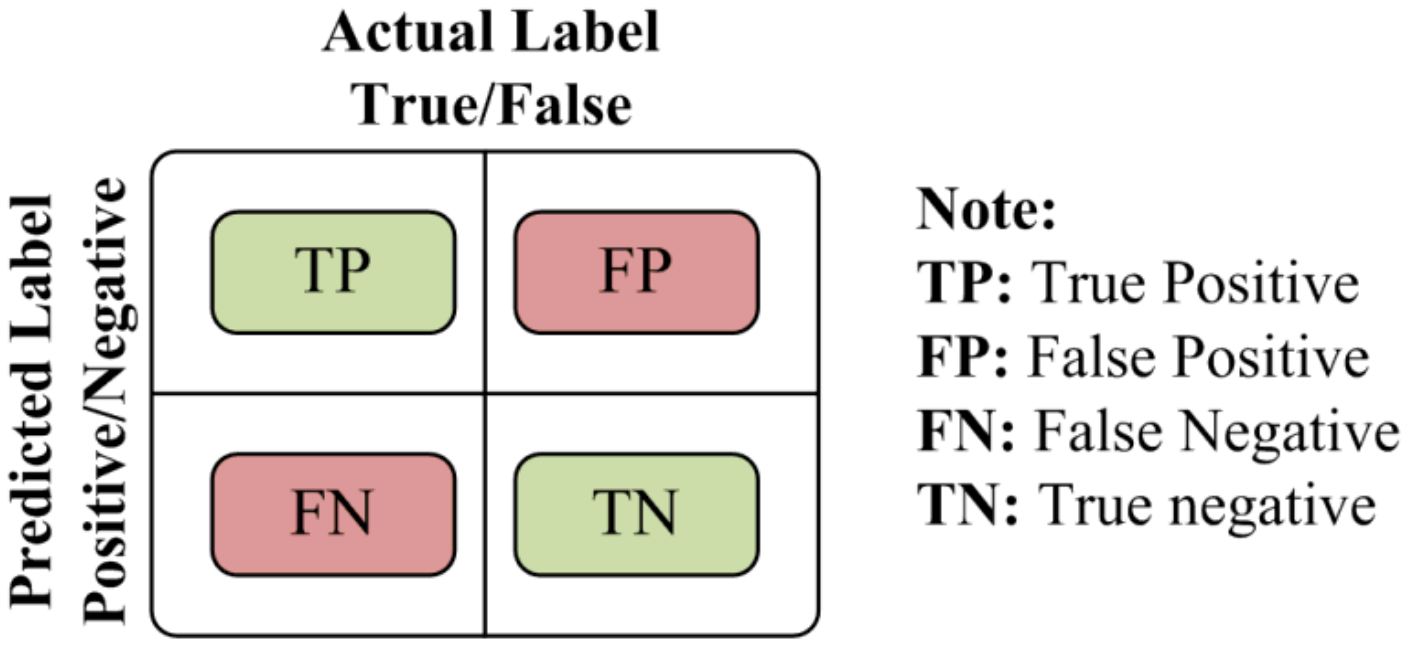

Figure 8

structure of confusion matrix

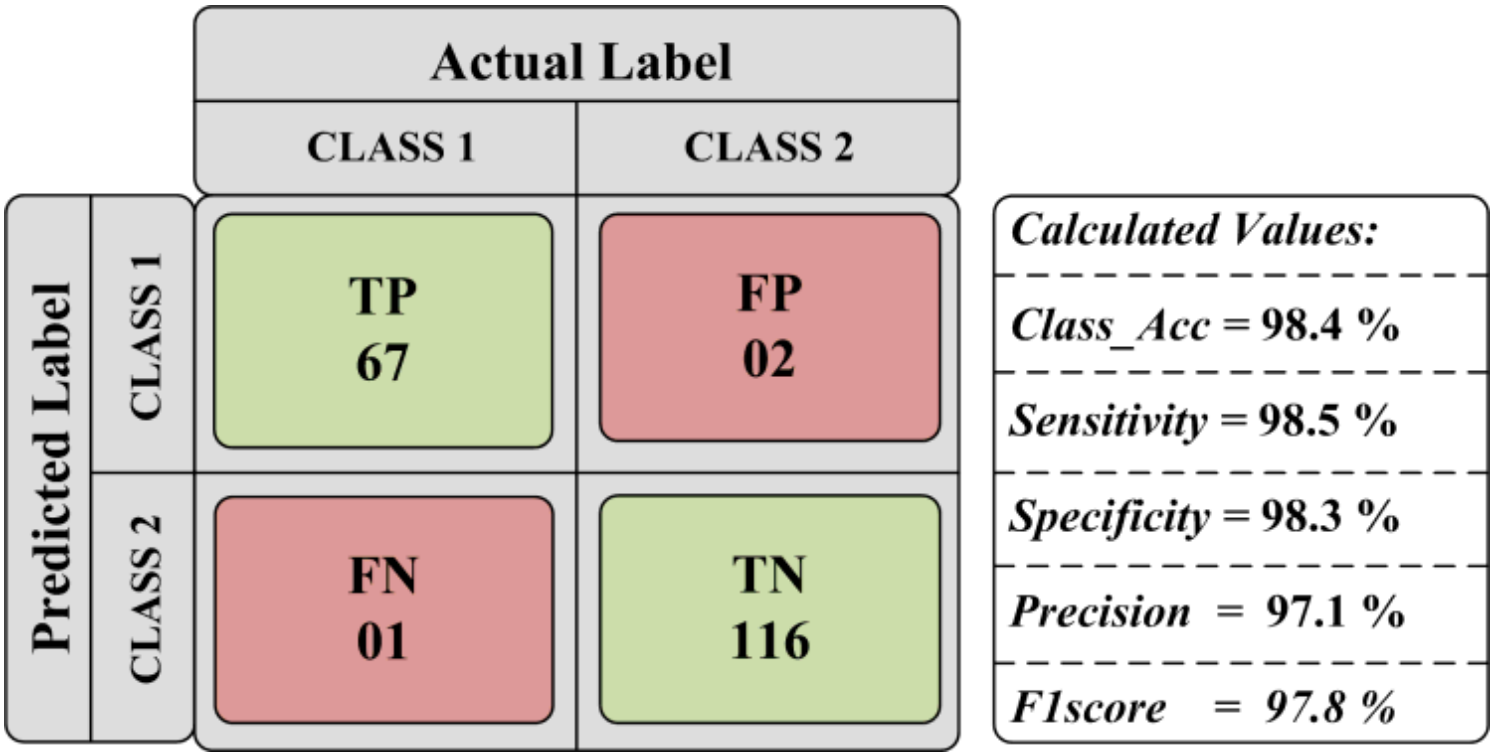

Figure 9

Obtained parametric value

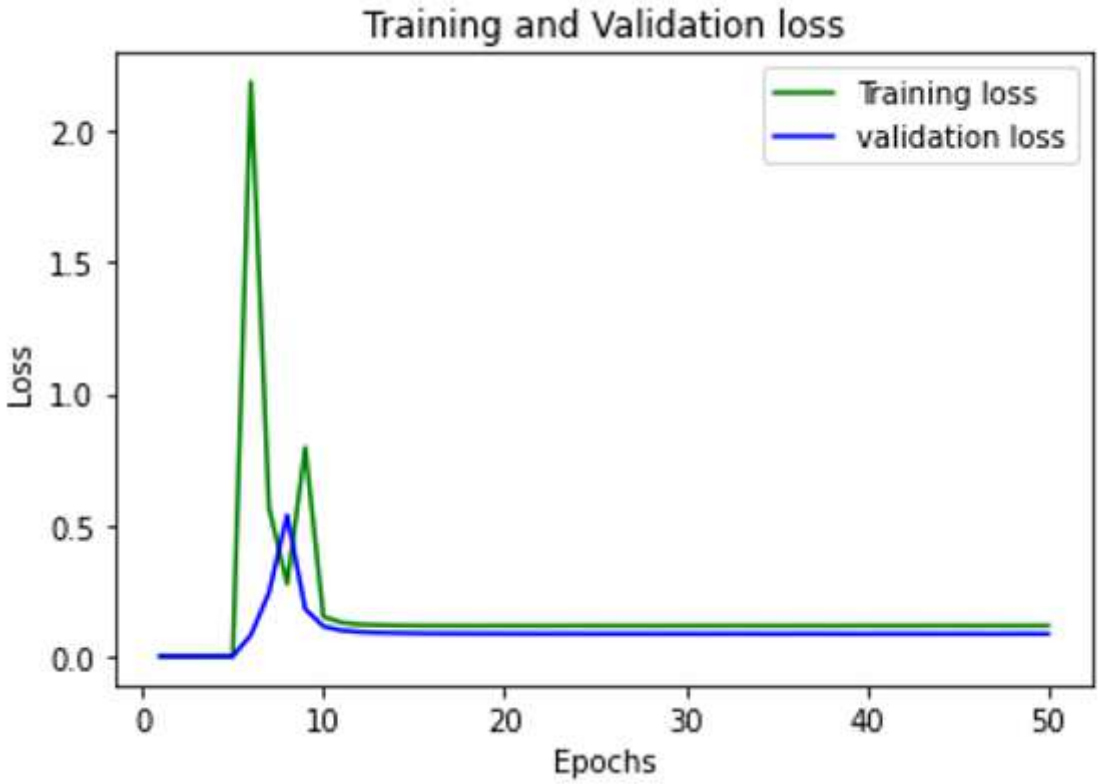

Figure 10

Performance Curve for Training vs. Validation Loss

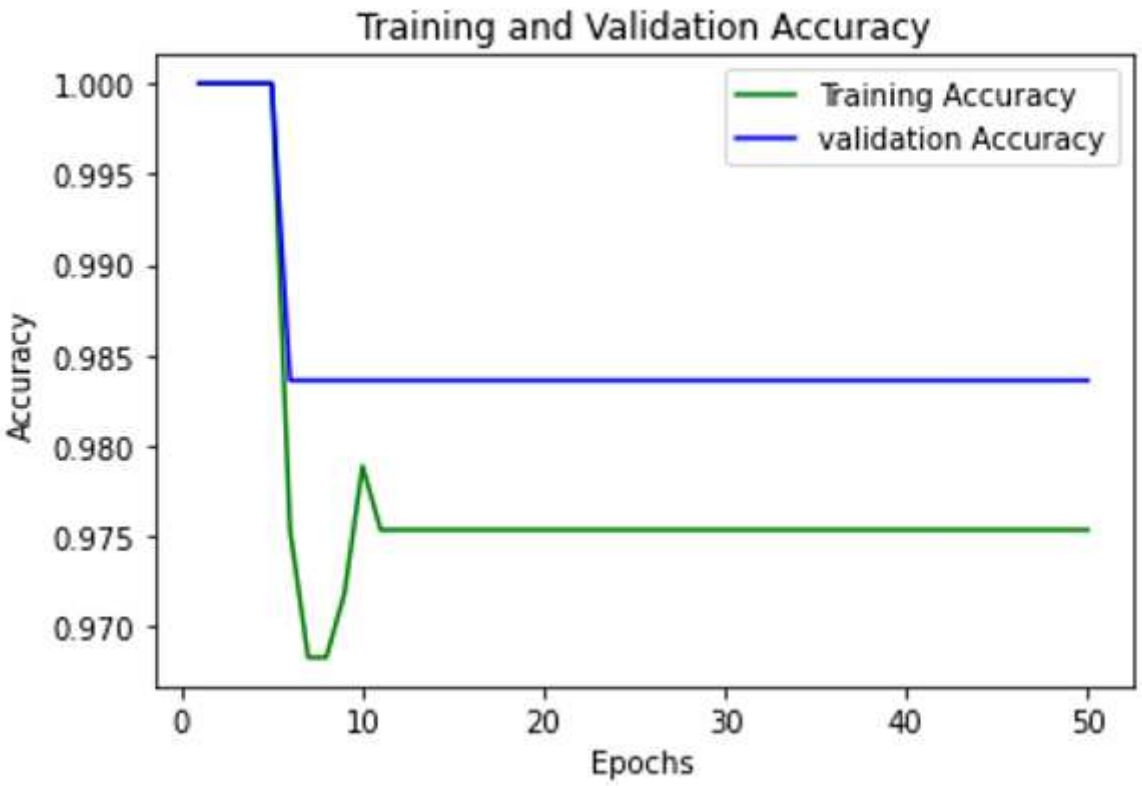

Figure 11

Performance Curve for Training vs. Validation Accuracy

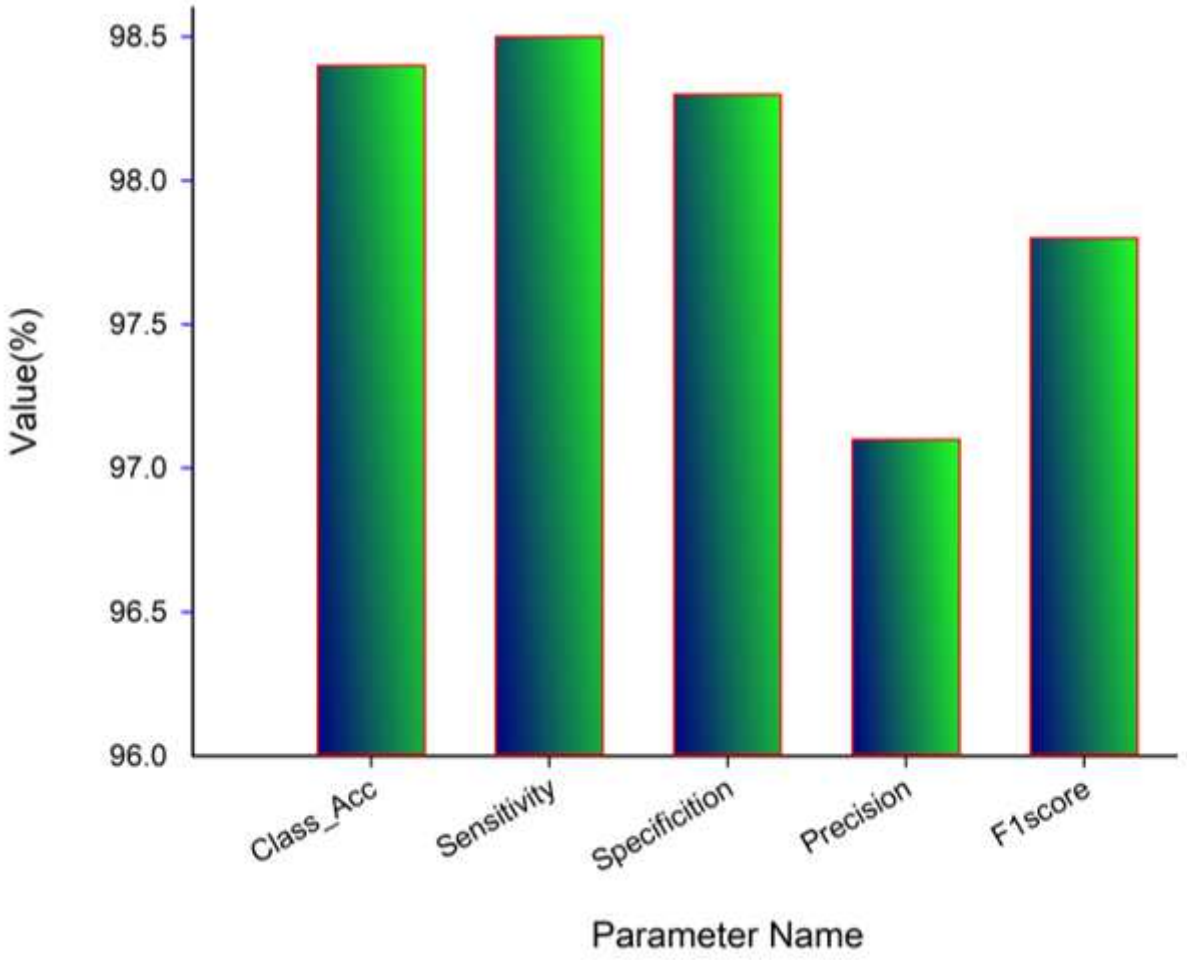

Figure 12

Quantitative Analysis of Proposed Work

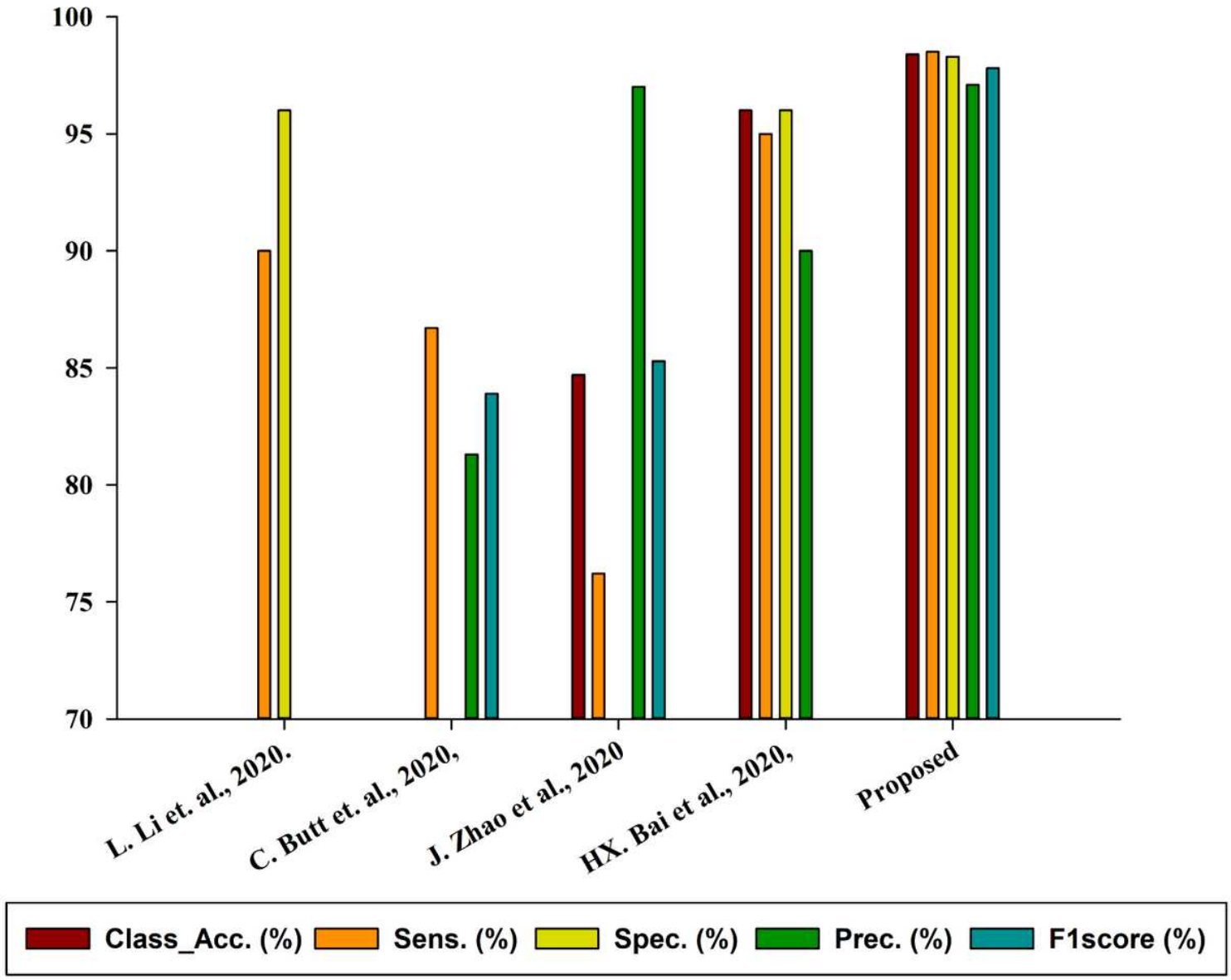

Figure 13

Comparative Analysis between Proposed Works with State-of-the-art.